Spin-orbit couplings within the equation-of-motion coupled-cluster framework: Theory, implementation, and benchmark calculations

Evgeny Epifanovsky, Kerstin Klein, Stella Stopkowicz, Jürgen Gauss, and Anna I. Krylov

Spin-orbit couplings within the equation-of-motion coupled-cluster framework: Theory, implementation, and benchmark calculations

Evgeny Epifanovsky,[1,2,3] Kerstin Klein,[4] Stella Stopkowicz,[5] Jürgen Gauss,[4] and Anna I. Krylov[1]

[1]*Department of Chemistry, University of Southern California, Los Angeles, California 90089-0482, USA*
[2]*Department of Chemistry, University of California, Berkeley, California 94720, USA*
[3]*Q-Chem Inc., 6601 Owens Drive, Suite 105, Pleasanton, California 94588, USA*
[4]*Institut für Physikalische Chemie, Universität Mainz, D-55099 Mainz, Germany*
[5]*Department of Chemistry, Centre for Theoretical and Computational Chemistry, University of Oslo, N-0315 Oslo, Norway*

We present a formalism and an implementation for calculating spin-orbit couplings (SOCs) within the EOM-CCSD (equation-of-motion coupled-cluster with single and double substitutions) approach. The following variants of EOM-CCSD are considered: EOM-CCSD for excitation energies (EOM-EE-CCSD), EOM-CCSD with spin-flip (EOM-SF-CCSD), EOM-CCSD for ionization potentials (EOM-IP-CCSD) and electron attachment (EOM-EA-CCSD). We employ a perturbative approach in which the SOCs are computed as matrix elements of the respective part of the Breit-Pauli Hamiltonian using zeroth-order non-relativistic wave functions. We follow the expectation-value approach rather than the response-theory formulation for property calculations. Both the full two-electron treatment and the mean-field approximation (a partial account of the two-electron contributions) have been implemented and benchmarked using several small molecules containing elements up to the fourth row of the periodic table. The benchmark results show the excellent performance of the perturbative treatment and the mean-field approximation. When used with an appropriate basis set, the errors with respect to experiment are below 5% for the considered examples. The findings regarding basis-set requirements are in agreement with previous studies. The impact of different correlation treatment in zeroth-order wave functions is analyzed. Overall, the EOM-IP-CCSD, EOM-EA-CCSD, EOM-EE-CCSD, and EOM-SF-CCSD wave functions yield SOCs that agree well with each other (and with the experimental values when available). Using an EOM-CCSD approach that provides a more balanced description of the target states yields more accurate results. © *2015 AIP Publishing LLC.* [http://dx.doi.org/10.1063/1.4927785]

I. INTRODUCTION

While it is not surprising that relativistic phenomena play a crucial role in the properties of heavy elements, the chemistry of molecules composed of light elements is also affected by relativity.[1,2] Among the various relativistic effects (orbital contraction, increase in binding energies, etc.), spin-orbit coupling (SOC) plays a special role. Although small in absolute magnitude (typical values of SOCs in organic molecules vary from several to hundreds of wave numbers), SOC facilitates the mixing of otherwise non-interacting states (e.g., singlet and triplet states); thus, it opens up new relaxation pathways for electronically excited states (via inter-system crossing, ISC) and enables new reaction channels.[1–3] For example, the reactions of O(^{3}P) or O$_2$($^3\Sigma_g^-$) with unsaturated hydrocarbons, which are common in combustion, proceed through triplet diradical formation[4–15] and the closed-shell singlet products can only be formed through ISC. Other examples of spin-forbidden processes in molecules composed of light elements involve reactions of N(^{4}S) and O(^{1}D).[16–20] Furthermore, SOCs are responsible for sensitization processes producing singlet oxygen, which is important in photochemistry[21–23] and is exploited in biomedical applications (e.g., in photodynamic therapy). SOC also gives rise to triplet emission (phosphorescence), which is essential in organic light-emitting devices.[24,25]

SOC is particularly important for open-shell species. For example, in doublet radicals with degenerate states (atoms in P, D, . . . states; linear molecules in Π, Δ, . . . states), SOC leads to a mixing of degenerate electronic configurations causing noticeable changes in the wave functions, energetics, and spectra. When chemical bonds are broken, SOC contributes to the non-parallelity error (and, consequently, errors in bond-dissociation energies), as it affects the most the energies of the open-shell products. Thus, accounting for SOC is essential for obtaining high-accuracy thermochemical data.[26]

SOC arises due to the coupling of the angular momentum of an electron with the intrinsic magnetic moment associated with its spin. For molecules composed of light atoms, relativistic effects can be accurately treated perturbatively by using the Breit-Pauli (BP) Hamiltonian.[27,28] Here, we are concerned with the spin-orbit part (spin-same-orbit and spin-

other-orbit terms) of the BP Hamiltonian,

$$H^{so} = \frac{\hbar e^2}{2m_e^2 c^2} \left[\sum_i \mathbf{h}^{so}(i) \cdot \mathbf{s}(i) - \sum_{i \neq j} \mathbf{h}^{soo}(i,j) \cdot (\mathbf{s}(i) + 2\mathbf{s}(j)) \right], \quad (1)$$

$$\mathbf{h}^{so}(i) = \sum_K \frac{Z_k(\mathbf{r}_i - \mathbf{R}_K) \times \mathbf{p}_i}{|\mathbf{r}_i - \mathbf{R}_K|^3} = \sum_K \frac{Z_K}{r_{iK}^3}(\mathbf{r}_{iK} \times \mathbf{p}_i), \quad (2)$$

$$\mathbf{h}^{soo}(i,j) = \frac{(\mathbf{r}_i - \mathbf{r}_j) \times \mathbf{p}_i}{|\mathbf{r}_i - \mathbf{r}_j|^3} = \sum \frac{1}{r_{ij}^3}(\mathbf{r}_{ij} \times \mathbf{p}_i), \quad (3)$$

where $\mathbf{r}_i$ and $\mathbf{p}_i$ are the coordinate and momentum operators of the ith electron and $\mathbf{R}_K$ and Z_K denote the coordinates and the charge of the Kth nucleus.

The first term, $\mathbf{h}^{so}(i)$, is a one-electron term; it originates from the electron-nuclear attraction. Since this term is proportional to the atomic charges, its magnitude increases significantly for heavy elements. The second term, $\mathbf{h}^{soo}(i,j)$, is a two-electron term. Its relative magnitude becomes less important for heavier elements, as here the one-electron part with its Z_k dependence dominates.[2,29] However, for organic molecules, the two-electron contribution to the total SOC is significant,[2,29] but fortunately can be accurately accounted for by a spin-orbit mean-field (called SOMF) approximation[2,30] as described below.

Fully relativistic schemes describe SOC in a natural manner. Here, we consider only SOC treatments within a non-relativistic framework using the BP Hamiltonian. Full SOC treatments and various flavors of the SOMF approximation have been implemented for different types of wave functions[1,29,31–39] including those obtained by complete active-space self-consistent field (CASSCF),[3,29,31–34] multi-reference configuration interaction (MRCI),[1,35] coupled-cluster (CC) response,[37] equation-of-motion CC (EOM-CC),[37,38] multi-reference CC (MRCC) via the Mk-MRCCSD formulation.[39,40] Density functional theory (DFT) implementations have also been reported.[36,41,42] In most of the studies within the CC/EOM-CC framework, a perturbative approach was used,[37–39] but a variational inclusion of SOC in the EOM-CCSD treatments was also recently presented.[43–45]

All previous studies (see Refs. 2 and 3 and references therein) consistently confirm the importance of the two-electron part of the SOC for light molecules, as well as the excellent performance of the SOMF and further, even more drastic approximations. Benchmark studies comparing mean-field and full SOC results for the EOM-CC wave functions have demonstrated that errors introduced by the mean-field approximation are much smaller than those due to other approximations.[37,38] The SOMF scheme has also been successfully used within other electronic-structure methods.[2,35,36] However, despite the success of the SOMF approximation, it is desirable to have a full two-electron treatment of SOC available. The SOMF scheme, for example, has not yet been thoroughly tested for organic diradicals, where the two-electron SO part is responsible for strongly geometry-dependent SOCs.[46,47]

This paper focuses on the calculation of SOCs within the EOM-CC framework thereby using the usual CCSD

approximation. EOM-CC provides an efficient and robust framework for computing multiple electronic states[48–54] and extends the single-reference CC methodology to multi-configurational wave functions. For example, EOM-EE (excitation energy) can describe multiple electronically excited states including situations where the states are of a strongly mixed character.[55] EOM-IP (ionization potential) and EOM-EA (electron attachment) enable the description of open-shell doublet states and charge-transfer systems.[56] EOM-SF (spin-flip) allows one to tackle diradicals, triradicals, and bond-breaking situations.[57] Thus, EOM-CC provides an attractive framework for the calculation of SOCs.

There are two ways to account for the spin-orbit effects:[2] a variational approach (in which the spin-orbit part of the BP Hamiltonian is included into the total Hamiltonian during the wave function computation, e.g., when solving CI, CC, or EOM-CC equations) and a perturbative approach. In the latter, which we adopt in this work, one first computes the non-relativistic wave functions and then evaluates the matrix elements of H^{so} between the states of interest (usually, for a small block of interacting states). Diagonalization of this Hamiltonian in the basis of the zero-order states yields the perturbed wave functions and the splittings that can be directly compared with experimental values. Thus, our target quantities are the matrix elements of H^{so} given by Eq. (1) between the non-relativistic wave functions, $\Psi(s, m_s)$ and $\Psi'(s', m_s')$, of the states involved,

$$\langle H^{so} \rangle = \langle H_x^{so} \rangle + \langle H_y^{so} \rangle + \langle H_z^{so} \rangle, \quad (4)$$

$$\langle H_\alpha^{so} \rangle \equiv \langle \Psi(s,m_s)|H_\alpha^{so}|\Psi'(s',m_s')\rangle, \quad \alpha = x, y, z. \quad (5)$$

Following the above equations, $\langle H^{so} \rangle$ is a complex number given by the sum of the matrix elements of the three Cartesian components of the spin-orbit operator from Eqs. (2) and (3).

Note that the couplings between different multiplet components, as well as the individual Cartesian contributions, are not invariant with respect to molecular orientation (assuming that the spin quantization axis is fixed along the z-axis). However, the quantity called SOC constant[3,33] (SOCC) is invariant,

$$|\text{SOCC}(s,s')|^2 \equiv \sum_{m_s=-s}^{s} \sum_{m_s'=-s'}^{s'} \left[\left| \langle \Psi(s,m_s)|H_x^{so}|\Psi'(s',m_s')\rangle \right|^2 \right.$$
$$+ \left| \langle \Psi(s,m_s)|H_y^{so}|\Psi'(s',m_s')\rangle \right|^2$$
$$+ \left. \left| \langle \Psi(s,m_s)|H_z^{so}|\Psi'(s',m_s')\rangle \right|^2 \right]. \quad (6)$$

The SOCC is useful in the context of Fermi's Golden Rule calculations of rates for spin-forbidden processes. Experimentally, SOCs are inferred from level splittings, intensity patterns, or rates; the exact relationship between the SOC matrix elements and spectroscopic observables depends on the system and states involved. Selection rules for SOCs are based on the Wigner–Eckart rules[58,59] and are discussed in detail in Ref. 3 (see also Appendix).

In this paper, we report an implementation for the calculation of SOCs using EOM-EE/SF/IP/EA-CCSD wave functions, including both a full two-electron SOC treatment

and the SOMF approximation. Using several small molecules, we benchmark the performance of these methods. The accuracy of the SOCs computed with EOM-CCSD wave functions is assessed by comparing the computed splittings with experimentally derived values and previously reported theoretical estimates. The accuracy of the SOMF approximation is evaluated by a comparison with results from full two-electron calculations. By using various flavors of EOM methods (e.g., EOM-EE versus EOM-SF, EOM-IP versus EOM-EA), we assess the impact of different zero-order wave functions on the computed values. Finally, by using open-shell references (such as in the SF methods), we investigate the impact of spin contamination on SOCs.

The structure of the paper is as follows. Section II presents the theory. We begin with a brief presentation of EOM-CCSD (Section II A) followed by a discussion of the formalism for calculating properties within the EOM framework (Section II B). We then introduce the BP Hamiltonian in its second-quantization form and discuss the calculation of the respective matrix elements (Section II C). Section II D presents the mean-field treatment of the two-electron spin-orbital part of the BP Hamiltonian. Details of the implementation are given in Section II E and in the appendices, while benchmark results are presented and discussed in Section III.

II. THEORY

A. Equation-of-motion coupled-cluster methods with single and double excitations

The EOM-CC approach provides an efficient and robust framework for computing multiple electronic states.[48–54] As described below, the different variants of the general EOM-CC formalism target different types of electronic states, such as electronically excited, electron-attached, or ionized states.[51] Some extensions of EOM-CC (such as the spin-flip and double ionization potential methods) facilitate the treatment of multi-configurational wave functions that appear, for example, in bond breaking and polyradicals.[57,60–69] The EOM-CC methods are closely related, or in some situations equivalent, to the linear-response CC approaches.[70–74]

The EOM-CC wave function has the following form:

$$|\Psi\rangle = Re^T|\Phi_0\rangle, \qquad (7)$$

where the linear EOM operator R acts on the reference CCSD wave function $e^T|\Phi_0\rangle$. The operator T is an excitation operator satisfying the reference-state CC equations,

$$\langle\Phi_\mu|\bar{H}|\Phi_0\rangle = 0, \qquad (8)$$

where Φ_μ are the μ-tuply excited determinants (with respect to the reference determinant[75] Φ_0) and $\bar{H} = e^{-T}He^T$ (the actual values of μ are determined by the level of truncation of T, e.g., $\mu = 1,2$ for CCSD). The EOM amplitudes R and the corresponding energies are found by diagonalizing the similarity-transformed Hamiltonian, $\bar{H}$, in the space of target configurations defined by the choice of the operator R and the reference Φ_0 (see Ref. 51 for a detailed description of different EOM models),

$$\bar{H}R = ER. \qquad (9)$$

In EOM-CCSD, the CC and EOM operators are truncated as follows:

$$T \approx T_1 + T_2, \qquad R \approx R_0 + R_1 + R_2, \qquad (10)$$

where only the single and double excitation operators (1-hole-1-particle ($1h1p$) and 2-holes-2-particles ($2h2p$)) are retained in T and R (in the case of EOM-EE and EOM-SF),

$$T_1 = \sum_{ia} t_i^a a^\dagger i \qquad T_2 = \frac{1}{4}\sum_{ijab} t_{ij}^{ab} a^\dagger b^\dagger ji, \qquad (11)$$

$$R_0 = r_0 \qquad R_1 = \sum_{ia} r_i^a a^\dagger i \qquad R_2 = \frac{1}{4}\sum_{ijab} r_{ij}^{ab} a^\dagger b^\dagger ji. \qquad (12)$$

In EOM-IP and EOM-EA, R is truncated at the $2h1p$ and $2p1h$ levels, respectively.

Since $\bar{H}$ is a non-Hermitian operator, its left and right eigenstates, $\langle\Phi_0|L$ and $R|\Phi_0\rangle$, are not identical but form a biorthogonal set,

$$\bar{H}R|\Phi_0\rangle = ER|\Phi_0\rangle, \qquad (13)$$

$$\langle\Phi_0|L\bar{H} = \langle\Phi_0|LE, \qquad (14)$$

$$\langle\Phi_0|L^M R^N|\Phi_0\rangle = \delta_{MN}, \qquad (15)$$

where M and N denote the Mth and Nth EOM states and

$$L = L_1 + L_2 = \sum_{ia} l_a^i i^\dagger a + \frac{1}{4}\sum_{ijab} l_{ab}^{ij} i^\dagger j^\dagger ba. \qquad (16)$$

The expansion coefficients, l_a^i, l_{ab}^{ij}, r_i^a, and r_{ij}^{ab}, are found by diagonalizing the corresponding matrix representation of $\bar{H}$. For energy calculations, the knowledge of the right eigenstate is sufficient. However, in property calculations, both the left and right eigenstate need to be computed. The r and l amplitudes are used to compute the one and two-particle transition-density matrices (DMs) defined below.

In addition to choosing different types of target states, one can also impose constraints on the spatial and spin symmetry of the EOM-CC operators thereby exploiting the block-diagonal structure of $\bar{H}$. Typically, only a minimal set of target states is computed. For example, in EOM-IP/EA using a closed-shell reference, one would usually compute only the $M_s = \frac{1}{2}$ target states, since the $M_s = -\frac{1}{2}$ states are exactly degenerate with the $M_s = \frac{1}{2}$ ones. In EOM-EE, one usually considers spin-conserving ($M_s = 0$) excitations and solves separately for different target $\langle S^2\rangle$-blocks (e.g., singlets and triplets in closed-shell systems). We note that spin-flipping excitations from a closed-shell reference produce the $M_s = \pm 1$ components of the triplet states that are degenerate with the $M_s = 0$ ones in EOM-EE. This is exploited in our implementation of SOC calculations — instead of deriving the $M_s = \pm 1$ transition-density matrices from those for $M_s = 0$ using the Wigner-Eckart rules, as done in other implementations,[35,76] we compute the $M_s = 1$ target states directly and use these wave functions to compute the respective density matrices. We also note that singlet-triplet SOCs can be computed by using an EOM-SF scheme in which the reference corresponds to a high-spin triplet state and the target low-spin states are obtained by spin-flip (e.g., $M_s = -1$) excitations.

B. Calculation of properties using approximate wave functions

There are two alternative strategies for computing properties and transition probabilities for approximate wave functions.[36,77] In the so-called response-theory formulation, one applies time-dependent perturbation theory (PT) to an approximate state (e.g., the CCSD wave function); in this approach, transition moments are defined as the residues of the respective response functions (and excitation energies as poles). Identical expressions for properties can be derived for the static perturbations using an analytic-derivative formalism.[52,78–80] In the expectation-value approach, one begins with expressions derived for exact states and then uses approximate wave functions to evaluate the respective matrix elements. The two approaches give the same answer for the exact states; however, the expressions for approximate states are in general different.[77] For example, one can compute transition-dipole moments for EOM-EE using the expectation-value approach; in this case, a so-called unrelaxed one-particle transition-density matrix will be used.[81] Alternatively, a full response derivation gives rise to expressions that include amplitude (and, optionally, orbital) relaxation terms; this is how the properties are computed within the linear-response formulation of CC theory. Numerically, the two approaches are rather similar,[77,78,82] although the expectation-value formulation of properties within EOM-CC is not size-intensive[83] (the deviations, however, are relatively small[84]). The response formulation can become singular in the cases of degenerate states,[37] whereas the expectation-value approach does not have such a problem. The differences between the two formulations for transition properties will be discussed in detail elsewhere. Here, we focus solely on the expectation-value approach. Thus, we compute the SOCs by using Eq. (5) and EOM-CC wave functions.

As was noted before,[81] the non-Hermitian nature of EOM-CC theory requires additional steps when computing interstate properties. The matrix element of an operator A between states Ψ_M and Ψ_N is defined as follows:

$$|A_{MN}| = \sqrt{\langle\Psi_M|A|\Psi_N\rangle\langle\Psi_N|A|\Psi_M\rangle}. \quad (17)$$

A_{MN} is independent of the choice of the norms of the left and right EOM states (the left and right EOM states are biorthogonal; however, the norms of the left or right vectors are not uniquely defined). Thus, Eq. (5) is modified accordingly. The phase of A_{MN} is discussed in Ref. 37 — whereas it is not uniquely defined, one can define the relative phases of different A_{MN} in a way that ensures that they are consistent at different geometries. Here, we follow the recommendation from Ref. 37 and use the sign of $\langle\Psi_M|A|\Psi_N\rangle$ to define the phase.

When computing matrix elements between different EOM states, e.g., between the EOM-IP/EA target states, $\Psi_{M,N}$ correspond to the left and right EOM states for states M and N. When using EOM-EE/SF, two different situations are possible. One may compute the SOCs between the two EOM-EE states (e.g., S_1 and T_1); this is similar to the situation described above. However, one may also consider the calculation of SOCs between the reference CCSD and the target EOM-CC

states (e.g., S_0 and T_1 in EOM-EE or T_1 and S_0 in EOM-SF). This requires calculating the so-called Λ-amplitudes that can be described as the left eigenstate of $\bar{H}$ corresponding to the CCSD reference state. Thus, in Eq. (17), one should use the left and right target EOM-CC state for one of the states, whereas the second state (corresponding to the CCSD reference) assumes the following form:

$$|\Psi_0\rangle = |\Phi_0\rangle \qquad \langle\Psi_0| = \langle\Phi_0|(1 + \Lambda_1 + \Lambda_2) \quad (18)$$

where $\Lambda_{1,2}$ has the same form as $L_{1,2}$ operators for the left EOM states, Eq. (16).

C. Breit-Pauli Hamiltonian in second-quantization form

The spin-orbit part of BP Hamiltonian (1) assumes the following form in its second-quantization representation (using atomic units):

$$H^{so} = \frac{1}{2c^2}\left[\sum_{p,q} I_{pq}\, p^\dagger q + \frac{1}{2}\sum_{p,q,r,s} J_{pqrs}\, p^\dagger q^\dagger sr\right], \quad (19)$$

$$I_{pq} = \langle\phi_p(1)|\mathbf{h}^{so}(1)\mathbf{s}(1)|\phi_q(1)\rangle, \quad (20)$$

$$J_{pqrs} = -\langle\phi_p(1)\phi_q(2)|\mathbf{h}^{soo}(1,2)(\mathbf{s}(1) + 2\mathbf{s}(2))|\phi_r(1)\phi_s(2)\rangle, \quad (21)$$

where $\phi_p(1) \equiv \phi_p(\mathbf{r}_1, \sigma_1)$ denotes the pth spin orbital.

The matrices I_{pq} and J_{pqrs} are anti-symmetric,

$$\begin{aligned} I_{pq} &= -I_{qp} \\ J_{pqrs} &= -J_{rspq}. \end{aligned} \quad (22)$$

In addition, the two-electron spin-orbit integrals have the following symmetry:

$$J_{pqrs} = -J_{rqps} = J_{psrq}. \quad (23)$$

Spin-symmetry and programmable expressions for the one- and two-electron integrals $I_{pq}^{\sigma_p\sigma_q}$ and $J_{pqrs}^{\sigma_p\sigma_q\sigma_r\sigma_s}$ are given in Appendix A.

To compute SOCs, one needs to contract these integrals with the respective transition-density matrices,

$$\langle\Psi(s,m_s)|H^{so}|\Psi'(s',m_s')\rangle = \sum_{pq} I_{pq}\gamma_{pq} + \frac{1}{2}\sum_{pqrs} J_{pqrs}\Gamma_{pqrs}, \quad (24)$$

where

$$\gamma_{pq} = \langle\Psi(s,m_s)|p^+q|\Psi'(s',m_s')\rangle, \quad (25)$$

$$\Gamma_{pqrs} = \langle\Psi(s,m_s)|p^+q^+sr|\Psi'(s',m_s')\rangle. \quad (26)$$

When using the SOMF approximation, only the one-particle DM is needed,

$$\langle\Psi(s,m_s)|H^{so}|\Psi'(s',m_s')\rangle \approx \sum_{pq} \mathbf{H}_{pq}^{SOMF}\gamma_{pq}, \quad (27)$$

where $\mathbf{H}_{pq}^{SOMF}$ is the effective one-electron spin-orbit operator described below.

Because the matrices I_{pq} and J_{pqrs} are anti-symmetric, the unsymmetrized (or anti-symmetrized) transition-density matrices need to be used to evaluate Eqs. (24) and (27),

which is different from the calculation of most other inter-state properties. The symmetric part of the DMs does not contribute to the computed SOC matrix elements. The expressions for the required DMs are given in the supplementary material.[85]

$$H^{SOMF} = \sum_{pq} \mathbf{H}^{SOMF}_{pq} p^\dagger q \tag{28}$$

$$\mathbf{H}^{SOMF}_{pq} = \langle \phi_p(1)|\mathbf{h}^{so}(1)\mathbf{s}(1)|\phi_q(1)\rangle + \frac{1}{2}\sum_r n_r[\langle \phi_p(1)\phi_r(2)|\mathbf{h}^{soo}(1,2)(\mathbf{s}(1)+2\mathbf{s}(2))|\phi_q(1)\phi_r(2)\rangle$$

$$- \langle \phi_p(1)\phi_r(2)|\mathbf{h}^{soo}(1,2)(\mathbf{s}(1)+2\mathbf{s}(2))|\phi_r(1)\phi_q(2)\rangle - \langle \phi_r(1)\phi_p(2)|\mathbf{h}^{soo}(1,2)(\mathbf{s}(1)+2\mathbf{s}(2))|\phi_q(1)\phi_r(2)\rangle]$$

$$= I_{pq} + \frac{1}{2}\sum_r n_r[J_{prqr} - J_{prrq} - J_{rpqr}], \tag{29}$$

where n_r is the average occupation of the rth spin orbital.

Eq. (29) can be written in a more general form[30,35] using an arbitrary (not necessarily diagonal) density matrix ρ_{rs},

$$\mathbf{H}^{SOMF}_{pq} = I_{pq} + \frac{1}{2}\sum_{rs} \rho_{rs}[J_{prqs} - J_{prsq} - J_{rpqs}]. \tag{30}$$

We use the symbol ρ here to distinguish this state-density matrix from the transition-density matrix γ defined above. We also note that ρ is a symmetric matrix.

The form of the SOMF operator has been introduced[30] by analyzing matrix elements between determinants that differ by one spin orbital. It was noted that the contributions from doubly occupied orbitals can be added up and that only the singly occupied orbitals need to be considered explicitly. Below, we present an alternative derivation.

The mean-field approximation can be derived by analyzing the contributions to the total matrix element of a two-electron operator from the separable and non-separable parts of the two-particle DM (2DM). Note that the treatment presented below applies for both state properties (expectation values) and inter-state matrix elements. In the latter case, transition 2DMs are employed.

The separable part of 2DM, $\tilde{\Gamma}$, in CC/EOM-CC has the following form:[86]

$$\tilde{\Gamma}_{pqrs} = \mathcal{P}_+(pr,qs)\mathcal{P}_-(p,q)\rho_{rp}\gamma_{qs}$$
$$= \rho_{rp}\gamma_{qs} - \rho_{rq}\gamma_{ps} + \rho_{sq}\gamma_{pr} - \rho_{sp}\gamma_{qr}, \tag{31}$$

$$\rho_{rp} = \begin{cases} \delta_{rp} & r,p \in \text{occupied in } \Phi_0 \\ 0 & \text{otherwise} \end{cases}. \tag{32}$$

When contracted with a two-electron operator, $A = \frac{1}{2}\sum_{pqrs} A_{pqrs}p^\dagger q^\dagger sr$, it yields the following contribution to the overall matrix element:[87]

$$\alpha^{2e} = \frac{1}{2}\sum_{pq}\gamma_{pq}\left[\sum_{rs}\rho_{rs}\left(A_{prqs} + A_{rpsq} - A_{prsq} - A_{rpqs}\right)\right]. \tag{33}$$

Further simplifications are possible depending on the permutational symmetry of the matrix A. For the SOC operator, see Eqs. (22)–(23), we thus obtain

D. Mean-field treatment of the two-electron spin-orbit part

The mean-field approximation[2,30] leads to the following effective spin-orbit Hamiltonian:[37,38]

$$\alpha^{2e} = \frac{1}{2}\sum_{pq}\gamma_{pq}\left[\sum_{rs}\rho_{rs}\left(J_{prqs} - J_{prsq} - J_{rpqs}\right)\right]. \tag{34}$$

This is exactly the mean-field expression given by Eq. (30). The spin-integrated expression for α^{2e} is given in Appendix B.

As evident from Eq. (34), this is a combined contribution from all the configurations in Ψ and Ψ' differing by one-electron excitation only. The value of this matrix element is bound by the norm of γ, $\|\gamma\|$, by virtue of the Cauchy-Schwartz inequality.[88,89] For interacting states that can be described as pure one-electron excitations relative to each other, $\|\gamma\|$ is one; for states that are doubly excited with respect to each other, $\|\gamma\|$ is zero. The contributions from the non-separable part of the 2DM are due to configurations that differ by two-electron excitations. Thus, the mean-field approximation of a matrix element of a two-electron operator entails considering only the contributions from the configurations that differ by a one-electron excitation. We note that in the Hartree Fock–configuration interaction singles (or Kohn-Sham–time-dependent DFT) treatment of the transition, the non-separable part of 2DM is exactly zero; thus, the mean-field expression gives in these cases the exact two-electron contribution.[36] In the case of state properties, the contributions from the non-separable 2DM only arise due to correlation, that is, for HF wave functions, the 2DM contains only the separable part.

This analysis explains the success of the mean-field approximation. Indeed, in typical SOC calculations, such as for the SOCs between S_0 and T_1 or S_1 and T_1 states in organic molecules or couplings between the two components of a doublet state (see Section III A), the interacting states can be described as singly excited with respect to each other (in other words, the transition between the two states has a significant one-electron character). This analysis also indicates when to expect a break-down of the mean-field approximation — when the two interacting states are doubly excited with respect to each other. In such a case, there are no contributions from the one-electron part and no contributions from the separable part, only the genuine (i.e., non-separable) two-electron contributions survive. Of course, in these situations, the anticipated magnitude of the SOC is small. To detect such

situations, one can monitor $\|\gamma\|$ — if its value becomes too low, one should consider computing the full two-electron SOC.

The mean-field expression given above is independent of whether one considers two or more states since the separable part of the 2DM has always the same form and the differences between the states are contained in γ. Therefore, there is no justification and no need for using state-averaged density matrices in Eq. (29).

The SOMF Hamiltonian can be used as a starting point for more drastic approximations. For example, by retaining only the diagonal blocks of ρ (in the AO basis), one arrives at the atomic mean-field (AMFI) approximation. A further cost reduction can be achieved by introducing one-center approximations for the one and two-electron integrals (AMFI approximation).[90]

E. Implementation

The expectation value of the SOC is computed in Q-Chem[91] by contracting the one- and two-electron SOC integrals with the appropriate transition-density matrices according to Eqs. (24) and (27). We compute the required target states by using general EOM-CCSD codes that allow to calculate the different M_s components of the triplet states by using spin-flipping operators. We use the following procedure for computing the full SOC:

1. Form the x, y, and z components of one- and two-electron SOC integrals in the AO basis by combining (geometric) second-derivative Coulomb integrals as prescribed in Ref. 32, see also Appendix.
2. For each EOM transition, compute the one- and two-particle transition DMs in the molecular spin-orbital basis.
3. Transform the appropriate spin blocks (see Appendix) of the DM into the AO basis; combine the transformed blocks to form the Cartesian components of the DM.
4. Contract the x, y, and z SOC integrals with the respective density matrices to yield the real and imaginary components of the SOC: $\langle H^{SO} \rangle = \langle H_y^{SO} \rangle + \langle H_x^{SO} \rangle + \langle H_z^{SO} \rangle$.
5. Repeat the procedure for the transposed counterpart of the EOM density matrix.
6. Evaluate the EOM average according to Eq. (17).

In order to obtain the SOC using the mean-field approximation, the two-electron SOC integrals are first contracted with the density matrix ρ_{rs} to form the matrix of the one-electron SOMF operator, see Eq. (34) and there the expression within the square brackets. In this case, the computation of the two-particle transition-density matrices is not required.

This implementation has been validated by comparing the computed SOCs against those obtained with the CFOUR[92] implementation. In CFOUR,[92] the SOC integrals are computed as described in Refs. 93 and 94 using the McMurchie-Davidson scheme.[95] The EOM-CC transition-density matrices have been computed using slightly modified versions of the available EOM-CC analytic-derivatives codes.[96–98] The obtained transition-density matrices are then transformed to the AO basis and contracted with the spin-orbit integrals. The SOMF scheme has been implemented based on the work in Refs. 40 and 94, noting that in Ref. 40, the mean-field scheme involves an additional averaging over spin.

III. RESULTS AND DISCUSSION

We begin the discussion by summarizing the results of previous calibration studies of SOCs calculations using CC/EOM-CC wave functions.[37–40] In Refs. 37–40, detailed benchmark calculations have been performed for diatomic and triatomic doublet radicals (OH, SH, SeH, ClO, BrO, NCS, N_2O^+, CCO^-, CCF, and CCCl) using EOM-IP-CCSD and Mk-MRCCSD wave functions.[38–40] Ref. 38 also considered O_2^+, CF, NO, PO, NS, and PS. In addition, the relative magnitude of the one- and two-electron contributions, the errors of the SOMF approximation versus a full two-electron treatment, the performance of the AMFI approximation, basis-set convergence, as well as different correlation treatments (EOM-IP-CCSD versus Mk-MRCCSD) have been investigated. In Ref. 37, the SOCs between S_0/T_1 and S_1/T_1 were analyzed using the response-theory formulation for the calculation of properties. The following molecules have been studied: BH, AlH, and HSiX (X = F, Cl, Br).

The most significant findings of these studies can be summarized as follows:[37–39]

1. In agreement with earlier studies (see Ref. 2 and references therein), the relative contribution of the two-electron part is large for light molecules (more than 50% of the one-electron part). The one- and two-electron contributions have opposite signs, so pure one-electron calculations significantly overestimate (by 50% and more) the coupling. In heavier molecules, the difference is less pronounced, but still noticeable (e.g., 25% and 10% in ClO and BrO, respectively).
2. The differences between the full two-electron treatment and the SOMF approximation are consistently small (usually less than 1 cm^{-1}) for both light and heavy molecules and are insensitive to the basis set.
3. Further approximations such as used in the AMFI approach introduce only minor errors.
4. The basis-set dependence of the SOCs in these species has been extensively investigated in Ref. 39 where basis sets up to cc-pCV5Z were used (with g, h, and i functions removed). In the case of Mk-MRCCSD wave functions with the SOMF approximation, the strongest basis-set dependence was observed for molecules with heavy atoms. For ClO, an increase of the basis set from cc-pCVDZ to cc-pCVTZ results in changes of about 10 cm^{-1} in the spin-orbit splitting, a further increase to quadruple and pentuple zeta leads to changes of 6 and 1 cm^{-1}, respectively. For light molecules, the differences are smaller, e.g., for OH, the difference between triple and quadruple zeta is less than 2 cm^{-1}. In Ref. 37, differences of less than 1% were observed for the SOCs computed with the aug-cc-pCVTZ and aug-cc-pVTZ basis sets in the case of BH.
5. In some cases, it was observed[37] that freezing the core electrons does not introduce large errors, i.e., differences less than 1 cm^{-1} between all-electron and valence-only calculations were reported in Ref. 37.
6. The differences between the EOM-IP-CCSD and Mk-MRCCSD values were found to be small (1%-3%).
7. For the set studied in Ref. 39, the errors of the computed SOCs were around 2%-10%. It was speculated that the

TABLE I. Spin-orbit splittings (cm^{-1}) in selected doublet radicals computed by EOM-IP-CCSD.[a]

Basis	OH			SH			SeH		
	1el	SOMF	1el+2el	1el	SOMF	1el+2el	1el	SOMF	1el+2el
cc-pVTZ/FC	210.12	135.62	134.23	419.80	338.05	337.78	1700.80	1535.28	1535.05
cc-pVTZ	210.21	135.68	134.27	445.17	359.40	358.98	1762.38	1591.61	1591.31
cc-pCVTZ/FC	211.21	136.51	135.10	418.48	336.97	336.72	1722.06	1554.03	1553.58
cc-pCVTZ	211.52	136.72	135.55	460.20	372.37	371.55	1859.42	1680.39	1679.37
cc-pVQZ/FC	210.30	136.26	134.96	413.56	333.02	332.78	1680.77	1516.97	1516.73
cc-pVQZ	210.50	136.40	135.13	439.09	354.34	353.92	1747.04	1577.55	1577.19
cc-pCVQZ/FC	211.20	137.04	135.74	415.11	334.40	334.17	1710.47	1543.60	1543.15
cc-pCVQZ	211.59	137.32	136.35	457.37	370.23	369.53	1857.34	1679.05	1677.94

[a]Functions with *g* and higher angular momentum omitted.

remaining discrepancy is due to the limitations of using non-relativistic zero-order wave functions and, possibly, higher-order correlation effects.

Below we consider several representative examples from previous studies, with an emphasis on using different zero-order wave functions. The following tight convergence thresholds were used in the Q-Chem calculations: SCF (10^{-12}), CCSD energy (10^{-10}), CCSD amplitudes (10^{-9}), EOM amplitudes (10^{-8}). In the Q-Chem calculations, *g* and higher angular-momentum functions were removed. In the CFOUR calculations, both the modified and unmodified basis sets were employed. Pure angular-momentum functions were used in all calculations.

A. EOM-CCSD calculations of SOCs in doublet radicals

Our first benchmark set comprises several $^2\Pi$ radicals for which experimental and theoretical values are available. As explained in Refs. 38–40, SOC leads to the mixing of the two degenerate components of the $^2\Pi$ state (Ψ_x and Ψ_y) resulting in the $\Pi_{1/2}$ and $\Pi_{3/2}$ states; the splitting between the two states equals $2 \cdot |\langle \Psi_x | H^{so} | \Psi_y \rangle|$, where only the z-component of $\langle H^{so} \rangle$ is non-zero.

We considered the following radicals: OH, SH, SeH, ClO, BrO, NCS, and N_2O^+. We used the same geometries as in Ref. 39 (the geometries and relevant energies are given in the supplementary material[85]).

The leading electronic configurations of Ψ_x and Ψ_y in OH, SH, and SeH are

$$\Psi_x = [core](\sigma)^2(\pi_x)^1(\pi_y)^2, \tag{35}$$

$$\Psi_y = [core](\sigma)^2(\pi_x)^2(\pi_y)^1. \tag{36}$$

These two states can be conveniently described by EOM-IP-CCSD using an anionic closed-shell reference state, $[core](\sigma)^2(\pi_x)^2(\pi_y)^2$. Alternatively, one can employ EOM-EE-CCSD in which one of the states is described by CCSD and the other by EOM-EE-CCSD. Yet, another possibility is to use EOM-EA-CCSD with a high-spin triplet reference, $[core](\sigma)^2(\pi_x)^1(\pi_y)^1$ (if the $\alpha\alpha$ reference state is used, the spin of the attached electron should be β). The EOM-IP-CCSD treatment is the most balanced, as both states are treated on the same footing and are spin-pure; also, the π_x

and π_y orbitals are exactly degenerate when using a closed-shell anionic reference. The relevant electronic states of ClO and BrO as well of NCS and N_2O are also best described by EOM-IP-CCSD using the appropriate closed-shell references.

Table I shows the results for OH, SH, and SeH computed with the polarized core-valence and the more compact cc-pVXZ basis sets with and without frozen core. We focus on the triple- and quadruple-zeta basis sets only (with *g* and higher angular-momentum functions removed), since the cc-pCVQZ results are essentially converged.[39] We observe that while freezing the core electrons has a negligible effect on the SOCs in OH; the errors for heavier elements are rather large (40-130 cm^{-1} in SeH, i.e., 3%-8%). Most of the error comes from the one-electron part of the SOC. Such a strong dependence on the core electrons is somewhat surprising, given that the relevant electronic states are more or less of valence Koopmans-like character. We note that this result is different from the findings reported in Ref. 37 where much smaller differences between all-electron and valence-only calculations have been observed for different systems and using a response-theory frozen-core treatment.

In the subsequent calculations, we employ the cc-pCVTZ basis for second and third row atoms and the cc-pCVQZ basis for heavier elements (with *g* and higher angular-momentum functions removed). For hydrogen, the cc-pVTZ basis is used. All electrons are correlated. We note that, based on the results from Table I, for molecules composed of second-row atoms, the cc-pVTZ basis can be employed in SOCs calculations with a frozen-core treatment.

Table II summarizes the splittings for the same set of radicals computed by different methods. The differences between the different EOM methods are small but noticeable; they range between 1% and 13% (the largest differences were observed for BrO and ClO, in other cases, the differences are 1% and 3%). We note that in all cases except SeH and N_2O, the EOM-IP-CCSD values are closer to the experimental ones, which is expected based on the more balanced description of the target states is provided by EOM-IP-CCSD. The states computed using an open-shell reference (as in the EOM-EA-CCSD and EOM-EE-CCSD calculations) might be affected by spin contamination.

The norms of the one-particle DMs reveal that the transitions between the states involved are indeed mostly of

TABLE II. Spin-orbit splittings (cm^{-1}) in selected doublet radicals computed by various EOM-CC methods.

| System | Expt. | IP-CCSD[a] | | | EA-CCSD[a,b] | | | EE-CCSD[a,b] | | | Mk-MRCCSD[c] | |
		1el+2el	SOMF	$\|\gamma\|$	1el+2el	SOMF	$\|\gamma\|$	1el+2el	SOMF	$\|\gamma\|$	1el+2el	SOMF
OH	139.2	135.55	136.72	0.98	135.57	132.77	0.97	136.08	134.73	0.96	135.1	136.1
SH	377.0	371.55	372.37	0.97	369.09	368.56	0.94	373.49	373.67	0.92	374.7	374.9
SeH	1764.4	1679.38	1680.40	0.97	1669.44	1669.03	0.94	1691.13	1691.56	0.93		
SeH/CQZ[d]		1677.94	1679.05	0.97	1682.51	1681.97	0.94	1708.12	1708.55	0.93	1707.6	1708.2
ClO	320.3	306.85	308.25	0.94	291.00	288.70	0.99	299.65	298.80	0.91	305.3	306.6
BrO	975.4	904.28	905.84	0.94	803.11	800.59	1.02	833.46	832.52	0.91		918.5
BrO/CQZ[d]		946.02	947.52	0.94	820.74	818.03	1.02	866.17	865.08	0.91		
NCS	325.3	329.90	330.68	0.94	336.28	335.54	0.93	338.79	338.83	0.89	360.4	
N$_2$O$^+$	132.4	126.91	127.73	0.94	130.70	128.47	0.93	129.25	128.22	0.89	130.9	

[a]cc-pCVTZ, all electrons are correlated.
[b]ROHF reference.
[c]Results from Ref. 39.
[d]cc-pCVQZ basis set with g and higher angular-momentum functions omitted, all electrons are correlated.

one-electron character ($\|\gamma\| \geq 0.89$). Interestingly, for these diatomic radicals, the EOM-IP-CCSD DMs show the largest one-electron character and the EOM-EA-CCSD ones the smallest.

Our second set consists of the isoelectronic doublet radicals from Ref. 38 — O$_2^+$, CF, NO, and several heavier ones (PO, NS, PS). The geometries are the same as in Ref. 38; they are given in the supplementary material.[85]

The two $^2\Pi$ states in these species have the following electronic configuration:

$$\Psi_x = [core](\sigma(s))^2(\sigma^*(s))^2(\sigma(p))^2(\pi_x)^2(\pi_y)^2(\pi_x^*)^1(\pi_y^*)^0, \quad (37)$$

$$\Psi_y = [core](\sigma(s))^2(\sigma^*(s))^2(\sigma(p))^2(\pi_x)^2(\pi_y)^2(\pi_x^*)^0(\pi_y^*)^1. \quad (38)$$

There are three possible ways to compute these states by EOM: (i) by EOM-EA using the closed-shell reference, $[core](\sigma(s))^2(\sigma^*(s))^2(\sigma(p))^2(\pi_x)^2(\pi_y)^2$, (ii) by EOM-IP using the high-spin reference, $[core](\sigma(s))^2(\sigma^*(s))^2(\sigma(p))^2(\pi_x)^2(\pi_y)^2(\pi_x^*)^1(\pi_y^*)^1$, as was done in Ref. 39, and (iii) by EOM-EE using either Ψ_x or Ψ_y as the reference.

Table III summarizes the results of these calculations. For CF, O$_2^+$, and NO, the difference between EOM-IP, EOM-EE, and EOM-EA does not exceed 6 cm^{-1} (about 3%). A similar trend is observed for the heavier species. The splittings computed with these methods agree with the experimental

values within ~3%. In almost all cases (except CF, PO and PS), the EOM-EA SOCs are closer to the experimental values than the SOCs computed by the other EOM models. This is expected, since EOM-EA provides the most balanced (and a spin-pure) description of the target states in these systems. We note that $\|\gamma\|$ are again close to one (≥ 0.87). For these systems, $\|\gamma\|$ for EOM-EA are the largest; this is expected based on the balanced nature of EOM-EA wave functions for these states. The EOM-EE-CCSD and EOM-IP-CCSD values in Table III are computed with a ROHF reference. To assess the impact of spin contamination due to the use of an open-shell reference, we repeated these calculations with a UHF (unrestricted HF) reference; the results are given in the supplementary material[85] (Table S6). One can see that the impact of choosing a UHF instead of a ROHF (restricted open-shell HF) reference is rather small in these systems (in most cases, the difference is less than 1 cm^{-1}); this is consistent with the relatively minor spin contamination of the reference (the deviation of $\langle S^2 \rangle$ from the exact values is 0.01-0.06). The largest observed difference between the results from ROHF and UHF based calculations is 7 cm^{-1} (EOM-EE calculations for PS); it also corresponds to the case with the largest spin contamination. We note that in this case, the ROHF value is closer to experiment; however, for NS in which the ROHF-UHF difference is 5 cm^{-1}, the situation is opposite.

TABLE III. Spin-orbit splittings (cm^{-1}) in selected doublet radicals computed by various EOM-CCSD methods using the cc-pCVTZ basis.

| System | Expt.[b] | EOM-EA | | | EOM-IP[a] | | | EOM-EE[a] | | |
		1el+2el	SOMF	$\|\gamma\|$	1el+2el	SOMF	$\|\gamma\|$	1el+2el	SOMF	$\|\gamma\|$
CF	77.1	76.37	74.93	0.97	78.15	79.11	0.94	77.00	76.48	0.92
O$_2^+$	200.3	204.31	201.37	0.97	193.84	195.27	0.90	195.13	193.70	0.88
NO	123.1	124.29	122.13	0.97	121.55	122.72	0.92	121.85	120.90	0.90
PO	224.0	233.04	232.21	0.95	215.67	216.53	0.92	223.87	223.76	0.89
NS	222.9	228.03	226.84	0.95	242.03	242.85	0.90	231.46	231.09	0.87
PS	321.9	330.50	330.01	0.94	327.55	328.35	0.91	327.92	328.11	0.87

[a]ROHF reference.
[b]Experimental values are taken from Ref. 38.

B. EOM-EE-CCSD and EOM-SF-CCSD calculations of SOCs between singlet and triplet states

Our next set comprises the closed-shell molecules studied in Ref. 37: BH, AlH, HSiF, HSiCl, and HSiBr. In these systems, we compute the SOCs between the S_0 and T_1 as well as the S_1 and T_1 states: $1^1\Sigma^+$ and $1^3\Pi$ for BH/AlH, and $1^1A'/1^1A''$ and $1^3A''$ for the triatomics. As described below, these target states can be accessed either by EOM-EE starting from a closed-shell reference, as was done in Ref. 37, or by EOM-SF-CCSD from a high-spin triplet reference. Thus, we can compare the impact of using different zero-order wave functions in these systems.

As explained in Appendix C, for the BH molecule in its standard orientation (along the z-axis), the coupling between the $M_s = 0$ component of the $1^3\Pi_x$ and $1^1\Sigma^+$ is zero and for the $M_s = \pm 1$ components, only $\langle H_x^{SO} \rangle$ is non-zero. By aligning the molecule along the x-axis, the coupling for the $M_s = \pm 1$ states becomes zero, but we compute a non-zero matrix element $\langle 1^1\Sigma^+ | H^{so} | ^3\Pi_x(m_s = 0) \rangle$ which is equal to $\langle H_z^{SO} \rangle$. The two matrix elements are not equal but connected by a factor of $\sqrt{2}$ that arises due to the wave-function normalization giving rise to the following relationship between the respective transition densities:

$$\|\gamma^{\alpha\alpha}(m_s = 0)\| = \|\gamma^{\beta\beta}(m_s = 0)\| = \frac{1}{\sqrt{2}}\|\gamma^{\alpha\beta}(m_s = -1)\|$$

$$= \frac{1}{\sqrt{2}}\|\gamma^{\beta\alpha}(m_s = 1)\|. \quad (39)$$

One can clearly see that the SOCC that entails summing over all multiplet components is invariant to the rotation,

$$\text{SOCC(along } z) = \sqrt{2} \times \langle H_x^{SO} \rangle = h_x, \quad (40)$$

$$\text{SOCC(along } x) = \langle H_z^{SO} \rangle = h_z. \quad (41)$$

These relationships provide an additional tool for validating the implementation.

The calculations were performed using the geometries from Ref. 37. We compare the use of EOM-EE versus EOM-SF wave functions. Table IV contains the results for AlH and BH computed with the cc-pCVTZ and aug-cc-pVTZ basis sets. We report the SOCC — see Eq. (40) and the discussion above. Reference 37 reported small differences between the results obtained with the aug-cc-pVTZ and aug-cc-pCVTZ basis sets. For BH, the difference was 3.48 versus 3.51 cm^{-1} (with core electrons kept frozen), whereas the all-electron calculations with aug-cc-pCVTZ gave 3.56 cm^{-1}. The difference between the LR-CCSD (linear response CCSD, i.e., response-theory formulation) and EOM-CCSD results is small (less than 2%). The effect of using a frozen core is small for BH, but for AlH, it is about 15%. The norms of $\|\gamma\|$ for the EOM-EE and EOM-SF transitions are similar in magnitude (0.9), which suggests that the description of the target states is of a similar quality by both methods. The differences between the EOM-EE and EOM-SF values are small (within 0.5%-2%).

We now proceed to the calculations for HSiX (X = F,Cl, Br), i.e., the silicon analogues of the halocarbenes. Table V lists the individual components of the SOC. The EOM-EE and EOM-SF values are within 4% from each other for the S_0-T_1 SOCs (EOM-reference); however, the differences for the T_1-

TABLE IV. Spin-orbit coupling constant (cm^{-1}) in BH and AlH computed with the SOMF approximation.

System	LR-CCSD[a]	EOM-EE-CCSD		EOM-SF-CCSD	
		SOCC	$\|\gamma\|$	SOCC	$\|\gamma\|$
BH/cc-pCVTZ		4.16	0.93	4.10	0.93
BH/aug-cc-pVTZ/FC[b]	3.48	4.01	0.93	3.96	0.93
BH/aug-cc-pVTZ		4.03	0.93	3.99	0.93
AlH/cc-pCVTZ		33.70	0.93	32.94	0.93
AlH/aug-cc-pVTZ/FC[b]	27.06	26.97	0.92	26.49	0.92
AlH/aug-cc-pVTZ		31.95	0.92	31.45	0.93

[a]Response-theory CCSD From. Ref. 37 using AMFI (SOMF + 1-center approximation for all spin-orbit integrals).
[b]In the frozen-core calculations, only 4 electrons are correlated.

S_1 couplings are much larger, up to 40%. The discrepancy is attributed to the poor performance of the current, non-spin-adapted version of EOM-SF for this particular type of interacting states, as explained in the following.

We note that spin contamination in the triplet reference is quite small for these molecules and the quality of the SF description of the target T_1, S_1, and S_0 states is good. The large difference between the EOM-EE and EOM-SF results for the S_1/T_1 SOCs originates from the nature of the SO operator that requires a change in the orbital orientation[47,99,100] (for example, the diagonal elements of the matrix representation of the one-electron part of the SO operator are zero). Consequently, the SOCs between states that have the same orbital occupations are small (this is known as the El-Sayed rule),[47,99] i.e., for a two-electron-in-two-orbitals system, the SOC between S_1 and T_1 will be nearly zero, whereas the SOC for S_0 and T_1 is not, as seen from Eqs. (A7)–(A9). In many-electron systems such as HSiX, the non-zero SOCs between $^1A''$ and $^3A''$ are due to the non-dominant electronic configurations (those not derived from HOMO-LUMO excitations) from the respective wave functions, whereas the SOC between the $^1A'$ and $^3A''$ states is due to the dominant configurations. As illustrated in Fig. 1, in the EOM-SF method together with a triplet reference, such leading ("diradical") configurations form a spin-complete set; however, other configurations (e.g., excitations from HOMO−1 to LUMO+1) sometimes miss the spin counterpart needed for a spin-complete description.[57,101] This results in a small residual spin contamination of the spin-flip target states. As one can see from the results for the S_0/T_1 couplings, this spin incompleteness apparently has only a relatively minor effect on the SOCs. However, since most of the non-zero contributions in the S_1/T_1 case are due to these configurations, the effect on the SOCs between these states is much more pronounced.

The differences between the EOM-CCSD and LR-CCSD values are small and vary between 4 and 15%. The difference is likely to be due to the use of different basis sets.

1. Spin-orbit couplings in diradical systems

Here, we consider several systems with a significant diradical character. We note that for these cases, the CCSD

TABLE V. Spin-orbit couplings (cm^{-1}) in HSiX (X=F,Cl,Br).[a]

System		LR-CCSD[b,c]		EOM-EE-CCSD[d]			EOM-SF-CCSD[d]		
		1el	SOMF	1el	SOMF	1el+2el	1el	SOMF	1el+2el
HSiF	$\langle 1^1A'|H_x^{so}|1^3A''\rangle$	59.82	45.14	68.11	51.60	51.56	65.61	49.73	49.69
	$\langle 1^1A'|H_y^{so}|1^3A''\rangle$	−29.52	−22.14	33.54	25.50	25.49	31.99	24.30	24.30
	SOCC($1^1A'/1^3A''$)	94.34	71.10	107.36	81.40	81.33	103.22	78.28	78.22
	$\langle 1^1A''|H_z^{so}|1^3A''\rangle$	8.04	6.01	8.12	6.22	6.17	6.51	5.02	5.00
HSiCl	$\langle 1^1A'|H_x^{so}|1^3A''\rangle$	75.17	59.38	85.85	67.86	67.79	81.93	64.74	64.67
	$\langle 1^1A'|H_y^{so}|1^3A''\rangle$	−47.12	−37.58	52.76	42.25	42.21	−51.28	−41.07	−41.04
	SOCC($1^1A'/1^3A''$)	125.47	99.38	142.51	113.05	112.93	136.68	108.43	108.32
	$\langle 1^1A''|H_z^{so}|1^3A''\rangle$	11.99	9.60	11.66	9.52	9.48	7.67	6.23	6.22
HSiBr	$\langle 1^1A'|H_x^{so}|1^3A''\rangle$	178.91	155.59	193.11	167.52	167.43	183.58	159.16	159.07
	$\langle 1^1A'|H_y^{so}|1^3A''\rangle$	−127.19	−111.77	137.00	120.27	120.22	−138.60	−121.84	−121.79
	SOCC($1^1A'/1^3A''$)	310.44	270.93	334.84	291.64	291.49	325.31	283.47	283.33
	$\langle 1^1A''|H_z^{so}|1^3A''\rangle$	66.36	59.42	62.22	56.07	56.02	37.11	33.37	33.35

[a]The Cartesian geometries from Ref. 37 were used (the individual components of SOCC are origin dependent).
[b]To obtain the $\langle H_x^{SO}\rangle$ and $\langle H_y^{SO}\rangle$ components, the values from Ref. 37 were divided by $\sqrt{2}$.
[c]From Ref. 37 using AMFI (SOMF + 1-center approximation for all spin-orbit integrals). LR-CCSD used ANO2 basis with all electrons correlated.
[d]cc-pCVTZ, all electrons correlated.

description of the reference is less satisfactory and the same also holds for the target EOM-EE states. This problem can easily be solved by using the EOM-SF method[57,60] in which one employs a well-behaved high-spin triplet reference.

We begin by considering several atoms with a triplet ground state (C, O, Si, and S). The EOM-EE-CCSD results are listed in Table VI. We compare the computed SOCCs against the values reported in Ref. 35 which were derived from the experimental data neglecting second-order effects. Despite the diradical character of the singlet states, the EOM-EE-CCSD SOCs are within 3% from the experimental values for O, Si. For C and S the difference is 12%. Unfortunately, we were not able to obtain EOM-SF results due to technical difficulties with the treatment of non-Abelian point-group symmetries.

In order to compare the EOM-SF with EOM-EE approach, we consider a set of methylene-like diradicals, CH_2, NH_2^+, SiH_2, and PH_2^+. We compute the SOCC, Eq. (6), between the $^3B_1$ and $^1A_1$ states at the equilibrium geometry of the triplet state. Note that these states differ in their orbital occupations and are expected to yield larger SOCs (by virtue of the El-Sayed rule[47,99]) than the $^3B_1$ and $^1B_1$ states (for the latter, the SOCC is exactly zero at the C_{2v} geometry due to symmetry, but can become non-zero if the symmetry is lowered to C_s). The results are summarized in Table VII. The differences between the EOM-EE and EOM-SF values range from 4%-5% (for SiH_2 and PH_2^+) to 24% (CH_2) and 102% (NH_2^+); the wave-function analysis reveals that the discrepancy correlates with the diradical character. For example, the weights of the second leading configuration in the EOM-SF
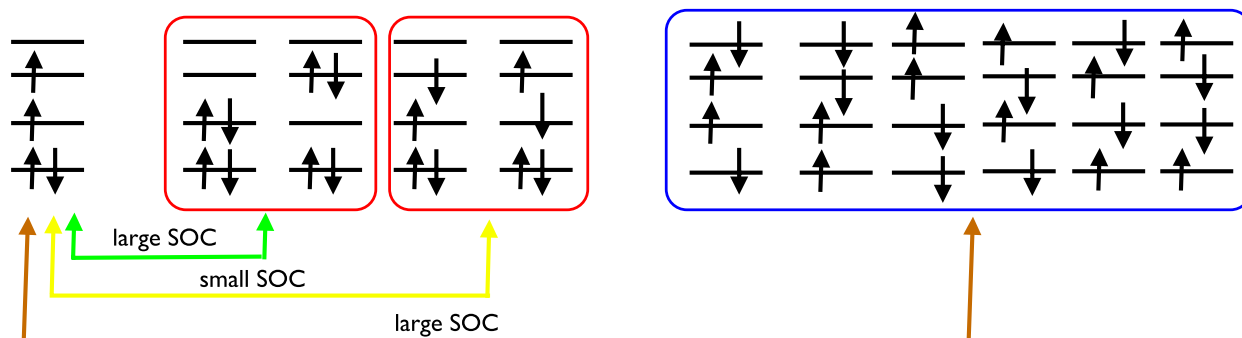

FIG. 1. Left: Electronic configuration of the triplet state used as a reference in SF calculations. The singly occupied orbitals of the triplet state define the singly occupied MO (SOMO) space; they correspond to the HOMO and LUMO orbitals in the closed-shell state. States derived from the HOMO-LUMO excitations (i.e., usually S_1 and T_1) as well as the closed-shell ground state are dominated by "primary" SF excitations (marked by red boxes). These configurations generated by excitations within the SOMO space form a spin-complete set even when only single excitations are included in the EOM ansatz. The excitations from doubly occupied orbitals to virtuals (marked by the blue box) include formally single (the first determinant in the blue box), double (determinants 2-4), and triple (the last determinant in the blue box) excitations from the high-spin triplet reference. Consequently, in standard SF calculations, these configurations do not form a spin-complete set. While their contribution to the S_0, S_1, and T_1 states is usually small, their effect on the respective SOCs varies. The SOC between the triplet state and the closed-shell determinants is large; therefore, it is dominated by primary SF configurations. However, the SOC between the open-shell singlet (S_1) and the T_1 state is expected to be small by virtue of the El-Sayed rule and is dominated by excitations outside the SOMO space.

TABLE VI. Absolute values of the SOCC (cm^{-1}) in selected ^3P atoms.

Method	C	O	Si	S
EOM-EE[a]/cc-pCVTZ	15.06	72.66	74.43	216.93
EOM-EE[a]/cc-pCVQZ[b]	15.63	79.49	76.19	220.60
Expt.[c]	13.98	77.40	73.70	194.62

[a]Obtained within the SOMF approximation.
[b]Functions with g and higher angular momentum omitted.
[c]From Ref. 35.

wave function of the $^1A_1$ states are 0.06 (CH$_2$), 0.25 (NH$_2^+$), and 0.01 (SiH$_2$ and PH$_2^+$). Thus, CCSD and EOM-EE are able to tackle single-configurational SiH$_2$ and PH$_2^+$ well. The quality of the description deteriorates for CH$_2$ with a moderate diradical character and is of unacceptable quality for NH$_2^+$ due to its even much more pronounced diradical character. The differences in the respective singlet-triplet gaps (EOM-EE versus EOM-SF) follow the same trend.[102] For CH$_2$ and SiH$_2$, the computed SOCCs can be compared with the results of previous calculations. Gordon and co-workers[3] reported MR-CISD values of 8.43 cm^{-1} and 39.34 cm^{-1}, respectively, using the WTBS basis (a heavily contracted unpolarized basis of a single-zeta quality).[103] Havlas *et al.* reported[100] CASSCF values of 12.40 cm^{-1} and 56.37 cm^{-1}. Thus, our results are in a semi-quantitative agreement with the other calculations.

In order to gain a better understanding of the performance of the EOM-EE and EOM-SF methods for diradicals, we also consider the halocarbene series,[104] HCX (X = F, Cl, and Br), for which SOCs derived from accurate experimental measurements have been recently reported.[105] The diradical character of the halocarbenes is less pronounced than for the parent methylene, i.e., their ground states are singlets, but the singlet-triplet gaps are small. The diradical character increases in the following series: HCF < HCBr < HCCl, as evidenced by the shrinking adiabatic singlet-triplet gap (from 0.6 eV in HCF to ~0.004 eV in HCBr).[104] The energy separation between the states varies strongly with the geometry, i.e., vertical singlet triplet gaps differ significantly from the adiabatic values. At the equilibrium triplet-state geometries, the vertical EOM-EE/SF singlet-triplet gaps are 0.121/0.127 eV, −0.320/−0.332 eV, and −0.379/−0.397 for HCF, HCCl, and HCBr, respectively (positive values mean that the singlet lies below the triplet state).

Table VIII presents the SOCC between the S$_0$ and T$_1$ states (S$_0$ is a closed-shell singlet state with a modest diradical character). The SOCCs are computed at the equilibrium geometries of the triplet states. We note that for HCF and HCCl, the deviations from the experimental values are almost the same for EOM-EE and EOM-SF, whereas for HCBr, EOM-EE-CCSD shows a slightly better agreement.

TABLE VII. Absolute values of the SOCC (cm^{-1}) between the $^3B_1$ and $^1A_1$ states in selected diradicals.[a]

Method	CH$_2$	NH$_2^+$	SiH$_2$	PH$_2^+$
EOM-SF[b]	7.82	13.01	48.53	100.82
EOM-EE[b]	9.66	26.10	50.76	104.92

[a]The SOCCs computed at the triplet-state equilibrium geometries from Ref. 102.
[b]Obtained within the SOMF approximation and with the cc-pCVTZ basis set.

TABLE VIII. Absolute values of the SOCCs (cm^{-1}) between the $^3A''$ and X^1A' states in HCX (X = F,Cl,Br).

Method	Basis	HCF	HCCl	HCBr
EOM-EE[a]	cc-pCVTZ	40.87	83.39	302.48
	cc-pCVQZ[b]	41.14	84.05	306.94
EOM-SF[a]	cc-pCVTZ	37.67	75.78	282.27
	cc-pCVQZ[b]	37.76	76.02	285.07
Expt.[105]		40[c]	81.3	350.9

[a]Obtained within the SOMF approximation.
[b]Functions with g and higher angular momentum omitted.
[c]Estimated by extrapolation.

IV. CONCLUSION

We presented the implementation of a scheme for the computation of SOCs within the EOM-CC theory. We employ a perturbative treatment in which the couplings are computed as matrix elements of the BP Hamiltonian using non-relativistic EOM-CC wave functions. We report both a full two-electron treatment of the SOC as well as the use of the SOMF approximation. The latter can be described as an incomplete treatment of the two-electron part of the SOC in which only the contributions from the separable part of the 2DM are considered. This is equivalent to taking into account only the contributions due to configurations in the interacting states that differ by the state of one electron. Since in most commonly considered cases (SOCs between the S$_0$-T$_1$ states, splittings in doublet radicals, etc.), the interacting states are indeed singly excited with respect to each other (which can be quantified by the norm of the one-particle transition DM[88,89]); this approximation works very well. Our implementation is based on the expectation-value approach to properties calculations rather than response theory.[77] We considered several examples focusing in particular on the impact of different correlation treatments on the SOCs. The main findings are as follows:

- The perturbative treatment of the SOC yields an excellent agreement with the experimental values even for systems with relatively heavy elements such as Br and Se (4th row) for which the errors in the computed SOCs were less than 5%. For lighter elements, the typical errors (in comparison to the experimentally derived values) are 1%-3%.
- In all cases, the SOMF approximation yields results within 1-3 cm^{-1} from those of a full two-electron treatment. One can monitor the norm of the one-particle transition DM, $\|\gamma\|$, in order to detect situations for which a full two-electron treatment may be required.
- The basis-set requirements for SOC calculations are more stringent than for energy calculations: quadruple-zeta basis sets give practically converged results; however, for 2nd and 3rd row elements, the use of a triple-zeta basis is sufficient. Polarized-core basis sets yield more accurate results; however, the performance of polarized-valence basis sets appears to be already reasonable.

- The treatment of core electrons may have an impact on the computed SOCs, even for states of predominantly valence character. We observed that freezing the core electrons may lead to errors around 10%-20% (SH, SeH, AlH). For molecules composed of second-row elements, however, the core electrons can be kept frozen in the correlation calculations.

- The correlation treatment in the underlying zero-order wave functions is important. We found that the EOM-IP-CCSD, EOM-EA-CCSD, EOM-EE-CCSD, and EOM-SF-CCSD wave functions yield SOCs which agree well with each other (and with the experimental values when available), provided that the target wave functions are well described by a given EOM model. As expected, using an EOM approach that yields a more balanced description of the target states yields more accurate results.

- In systems with significant diradical character, the choice of the appropriate EOM-CC method requires careful considerations. The EOM-EE and EOM-SF values for the SOCs in such systems can differ by a factor of 2. While EOM-SF usually yields a better description of the diradical wave functions, the quality of the SOC depends on the type of the states involved. For the couplings between a closed-shell type and triplet state in molecules with moderate diradicaloid character, both methods yield very similar results. When there is a very strong diradical character, the EOM-SF method is superior to EOM-EE. However, for the couplings between states of similar orbital configuration (i.e., for the transitions violating the El-Sayed rule[99]), such as T_1 and S_1 derived by a HOMO-LUMO excitation or triplet and open-shell singlet states in diradicals, EOM-SF is inferior to EOM-EE. We anticipate that this problem can be fixed by making the EOM-SF set of target configurations spin complete.

- The effect of spin contamination when using an open-shell reference in the EOM treatment is small. The errors of EOM-CCSD SOCs computed using an open-shell reference were of the same magnitude (~3%) as when calculated using a closed-shell reference. The use of a UHF instead of a ROHF reference does not have a considerable impact in cases of a moderate spin contamination of UHF wave functions.

APPENDIX A: EXPRESSIONS FOR SPIN-ORBITAL INTEGRALS

1. One-electron Breit-Pauli integrals

To derive programmable expressions for spin-orbit integrals, it is convenient to employ ladder and projection operators,

$$
\begin{aligned}
\mathbf{h}^{so}(j) \cdot \mathbf{s}(j) &= \sum_K \frac{Z_K}{r_{jK}^3} (\mathbf{r}_{jK} \times \mathbf{p}_j) \cdot \mathbf{s}(j) \\
&= \sum_K \frac{1}{2} L_+(j,K) s_-(j), \\
&\quad + \frac{1}{2} L_-(j,K) s_+(j) + L_z(j,K) s_z(j) \quad (A1)
\end{aligned}
$$

where

$$
L_+(j,K) \equiv \frac{Z_K}{r_{jK}^3} \left\{ [\mathbf{r}_{jK} \times \mathbf{p}_j]_x + i [\mathbf{r}_{jK} \times \mathbf{p}_j]_y \right\}, \quad (A2)
$$

$$
L_-(j,K) \equiv \frac{Z_K}{r_{jK}^3} \left\{ [\mathbf{r}_{jK} \times \mathbf{p}_j]_x - i [\mathbf{r}_{jK} \times \mathbf{p}_j]_y \right\}, \quad (A3)
$$

$$
L_z(j,K) \equiv \frac{Z_K}{r_{jK}^3} [\mathbf{r}_{jK} \times \mathbf{p}_j]_z, \quad (A4)
$$

and

$$
s_x = \frac{1}{2}\begin{pmatrix} 0 & 1 \\ 1 & 0 \end{pmatrix}, \qquad s_y = \frac{1}{2}\begin{pmatrix} 0 & -i \\ i & 0 \end{pmatrix},
$$

$$
s_z = \frac{1}{2}\begin{pmatrix} 1 & 0 \\ 0 & -1 \end{pmatrix}, \quad (A5)
$$

$$
s_+(j) \equiv s_x(j) + i s_y(j), \qquad s_-(j) \equiv s_x(j) - i s_y(j). \quad (A6)
$$

By performing spin integration, we can write the contributions from each L component in the basis of molecular spin-orbitals to each spin block of the SOC integrals,

$$
\begin{aligned}
&\begin{bmatrix} \langle \phi_p^\alpha | L_z | \phi_q^\alpha \rangle & \langle \phi_p^\alpha | \frac{L_-}{2} | \phi_q^\beta \rangle \\ \langle \phi_p^\beta | \frac{L_+}{2} | \phi_q^\alpha \rangle & -\langle \phi_p^\beta | L_z | \phi_q^\beta \rangle \end{bmatrix} \\
&= \frac{1}{2}\begin{bmatrix} 0 & \langle \phi_p^\alpha | L_x | \phi_q^\beta \rangle \\ \langle \phi_p^\beta | L_x | \phi_q^\alpha \rangle & 0 \end{bmatrix} \\
&\quad + \frac{1}{2}\begin{bmatrix} 0 & -i\langle \phi_p^\alpha | L_y | \phi_q^\beta \rangle \\ i\langle \phi_p^\beta | L_y | \phi_q^\alpha \rangle & 0 \end{bmatrix} \\
&\quad + \frac{1}{2}\begin{bmatrix} \langle \phi_p^\alpha | L_z | \phi_q^\alpha \rangle & 0 \\ 0 & -\langle \phi_p^\beta | L_z | \phi_q^\beta \rangle \end{bmatrix}.
\end{aligned}
$$

Thus, the Cartesian components of the one-electron part of the SOC operator can be written as follows:

$$
h_z^{1e} = \frac{1}{2} \sum_{pq} \left(L_{pq}^{z,\alpha\alpha} \gamma_{pq}^{\alpha\alpha} - L_{pq}^{z,\beta\beta} \gamma_{pq}^{\beta\beta} \right), \quad (A7)
$$

$$
h_x^{1e} = \frac{1}{2} \sum_{pq} \left(L_{pq}^{x,\alpha\beta} \gamma_{pq}^{\alpha\beta} + L_{pq}^{x,\beta\alpha} \gamma_{pq}^{\beta\alpha} \right), \quad (A8)
$$

$$
h_y^{1e} = -\frac{i}{2} \sum_{pq} \left(L_{pq}^{y,\alpha\beta} \gamma_{pq}^{\alpha\beta} - L_{pq}^{y,\beta\alpha} \gamma_{pq}^{\beta\alpha} \right). \quad (A9)
$$

To express $\langle\phi_p|L_{\{+-z\}}(K)|\phi_q\rangle$, we need

$$L_+(K) \equiv \frac{Z_K}{r_K^3}\left\{[\vec{r}_K\times\vec{p}]_x + i[\vec{r}_K\times\vec{p}]_y\right\}$$
$$= \frac{Z_K}{i}\left[\left(\frac{y-y_K}{r_K^3}\frac{\partial}{\partial z} - \frac{z-z_K}{r_K^3}\frac{\partial}{\partial y}\right)\right.$$
$$\left. + i\left(\frac{z-z_K}{r_K^3}\frac{\partial}{\partial x} - \frac{x-x_K}{r_K^3}\frac{\partial}{\partial z}\right)\right], \quad \text{(A10)}$$

$$L_-(K) \equiv \frac{Z_K}{r_K^3}\left\{[\vec{r}_K\times\vec{p}]_x - i[\vec{r}_K\times\vec{p}]_y\right\}$$
$$= \frac{Z_K}{i}\left[\left(\frac{y-y_K}{r_K^3}\frac{\partial}{\partial z} - \frac{z-z_K}{r_K^3}\frac{\partial}{\partial y}\right)\right.$$
$$\left. - i\left(\frac{z-z_K}{r_K^3}\frac{\partial}{\partial x} - \frac{x-x_K}{r_K^3}\frac{\partial}{\partial z}\right)\right], \quad \text{(A11)}$$

$$L_z(K) \equiv \frac{Z_K}{r_K^3}[\vec{r}_K\times\vec{p}]_z$$
$$= \frac{Z_K}{i}\left(\frac{x-x_K}{r_K^3}\frac{\partial}{\partial y} - \frac{y-y_K}{r_K^3}\frac{\partial}{\partial x}\right). \quad \text{(A12)}$$

To evaluate the above expressions, the following integrals are needed:

$$\left\langle\phi_p\left|\frac{u-u_K}{r_K^3}\frac{\partial}{\partial v}\right|\phi_q\right\rangle, \quad u,v = \{x,y,z\}. \quad \text{(A13)}$$

The required integrals can be computed using the McMurchie-Davidson scheme.[95] In the Q-Chem[91] implementation, we reused the code for second geometrical derivative Coulomb integrals as prescribed in Ref. 32.

Details for the implementation of the one-electron spin-orbital integrals within the CFOUR program package[92] can be found in Refs. 93 and 94. We only note here that this implementation follows closely Ref. 95 without use of ladder and projection operator techniques. The integrals are furthermore evaluated directly without computing geometrical integral derivatives as intermediates.

2. Two-electron Breit-Pauli integrals

The two-electron part of SOC can be tackled in a similar way,

$$h^{soo}(j,k)\cdot[s(j) + 2s(k)]$$
$$= \frac{1}{r_{jk}^3}(\vec{r}_{jk}\times\vec{p}_j)\cdot[s(j) + 2s(k)]$$
$$= J_+(j,k)\,[s_-(j) + 2s_-(k)] + J_z(j,k)\,[s_z(j) + 2s_z(k)]$$
$$+ J_-(j,k)\,[s_+(j) + 2s_+(k)], \quad \text{(A14)}$$

where the following ladder and projection operators were used:

$$J_+(j,k) \equiv \frac{1}{r_{jk}^3}\left\{[\vec{r}_{jk}\times\vec{p}_j]_x + i[\vec{r}_{jk}\times\vec{p}_j]_y\right\}, \quad \text{(A15)}$$

$$J_-(j,k) \equiv \frac{1}{r_{jk}^3}\left\{[\vec{r}_{jk}\times\vec{p}_j]_x - i[\vec{r}_{jk}\times\vec{p}_j]_y\right\} \quad \text{(A16)}$$

$$J_z(j,k) \equiv \frac{1}{r_{jk}^3}[\vec{r}_{jk}\times\vec{p}_j]_z, \quad \text{(A17)}$$

$$s_+(j) \equiv \frac{1}{2}[s_x(j) + is_y(j)], \qquad s_-(j) \equiv \frac{1}{2}[s_x(j) - is_y(j)]. \quad \text{(A18)}$$

This yields

$$J_{pqrs}^{\alpha\alpha\alpha\alpha} = \frac{3}{2}\langle\phi_p\phi_q|J_z|\phi_r\phi_s\rangle, \quad \text{(A19)}$$

$$J_{pqrs}^{\alpha\alpha\alpha\beta} = \langle\phi_p\phi_q|J_-|\phi_r\phi_s\rangle, \quad \text{(A20)}$$

$$J_{pqrs}^{\alpha\alpha\beta\alpha} = \frac{1}{2}\langle\phi_p\phi_q|J_-|\phi_r\phi_s\rangle, \quad \text{(A21)}$$

$$J_{pqrs}^{\alpha\alpha\beta\beta} = 0, \quad \text{(A22)}$$

$$J_{pqrs}^{\alpha\beta\alpha\alpha} = \langle\phi_p\phi_q|J_+|\phi_r\phi_s\rangle, \quad \text{(A23)}$$

$$J_{pqrs}^{\alpha\beta\alpha\beta} = -\frac{1}{2}\langle\phi_p\phi_q|J_z|\phi_r\phi_s\rangle, \quad \text{(A24)}$$

$$J_{pqrs}^{\beta\alpha\beta\alpha} = \frac{1}{2}\langle\phi_p\phi_q|J_z|\phi_r\phi_s\rangle, \quad \text{(A25)}$$

$$J_{pqrs}^{\alpha\beta\beta\alpha} = 0, \quad \text{(A26)}$$

$$J_{pqrs}^{\alpha\beta\beta\beta} = \frac{1}{2}\langle\phi_p\phi_q|J_-|\phi_r\phi_s\rangle, \quad \text{(A27)}$$

$$J_{pqrs}^{\beta\beta\beta\beta} = -\frac{3}{2}\langle\phi_p\phi_q|J_z|\phi_r\phi_s\rangle. \quad \text{(A28)}$$

Finally, it is convenient to write down the expressions for the Cartesian components of the two-electron SOC operator,

$$g_x = 2J_{pqrs}^{\alpha\alpha\alpha\beta} + J_{pqrs}^{\alpha\alpha\beta\alpha} + 2J_{pqrs}^{\alpha\beta\alpha\alpha} + J_{pqrs}^{\alpha\beta\beta\beta}$$
$$+ J_{pqrs}^{\beta\alpha\alpha\alpha} + 2J_{pqrs}^{\beta\alpha\beta\beta} + J_{pqrs}^{\beta\beta\beta\alpha} + 2J_{pqrs}^{\beta\beta\beta\alpha}, \quad \text{(A29)}$$

$$g_y = -i[2J_{pqrs}^{\alpha\alpha\alpha\beta} + J_{pqrs}^{\alpha\alpha\beta\alpha} - 2J_{pqrs}^{\alpha\beta\alpha\alpha} + J_{pqrs}^{\alpha\beta\beta\beta}$$
$$+ J_{pqrs}^{\beta\alpha\alpha\alpha} + 2J_{pqrs}^{\beta\alpha\beta\beta} - J_{pqrs}^{\beta\beta\beta\alpha} - 2J_{pqrs}^{\beta\beta\beta\alpha}], \quad \text{(A30)}$$

$$g_z = 3J_{pqrs}^{\alpha\alpha\alpha\alpha} - J_{pqrs}^{\alpha\beta\alpha\beta} + J_{pqrs}^{\beta\alpha\beta\alpha} - 3J_{pqrs}^{\beta\beta\beta\beta}]. \quad \text{(A31)}$$

Expansion of J in $\langle\phi_p\phi_q|J_{\{+-z\}}(1,2)|\phi_r\phi_s\rangle$,

$$J_+(1,2) \equiv \frac{1}{r_{12}^3}\left\{[\vec{r}_{12}\times\vec{p}_1]_x + i[\vec{r}_{12}\times\vec{p}_1]_y\right\}$$
$$= \frac{1}{i}\left[\left(\frac{y_1-y_2}{r_{12}^3}\frac{\partial}{\partial z_1} - \frac{z_1-z_2}{r_{12}^3}\frac{\partial}{\partial y_1}\right)\right.$$
$$\left. + i\left(\frac{z_1-z_2}{r_{12}^3}\frac{\partial}{\partial x_1} - \frac{x_1-x_2}{r_{12}^3}\frac{\partial}{\partial z_1}\right)\right], \quad \text{(A32)}$$

$$J_-(1,2) \equiv \frac{1}{r_{12}^3}\left\{[\vec{r}_{12}\times\vec{p}_1]_x - i[\vec{r}_{12}\times\vec{p}_1]_y\right\}$$
$$= \frac{1}{i}\left[\left(\frac{y_1-y_2}{r_{12}^3}\frac{\partial}{\partial z_1} - \frac{z_1-z_2}{r_{12}^3}\frac{\partial}{\partial y_1}\right)\right.$$
$$\left. - i\left(\frac{z_1-z_2}{r_{12}^3}\frac{\partial}{\partial x_1} - \frac{x_1-x_2}{r_{12}^3}\frac{\partial}{\partial z_1}\right)\right], \quad \text{(A33)}$$

$$J_z(1,2) \equiv \frac{1}{r_{12}^3}[\vec{r}_{12}\times\vec{p}_1]_z$$
$$= \frac{1}{i}\left(\frac{x_1-x_2}{r_{12}^3}\frac{\partial}{\partial y_1} - \frac{y_1-y_2}{r_{12}^3}\frac{\partial}{\partial x_1}\right). \quad \text{(A34)}$$

Thus, the following integrals are needed:

$$\int d1 \, d2 \, \phi_p(1)\phi_q(2) \frac{u_1 - u_2}{r_{12}^3} \frac{\partial \phi_r(1)}{\partial v_1} \phi_s(2). \quad (A35)$$

The required integrals can be computed using the McMurchie-Davidson scheme.[95] In the Q-Chem implementation, we reused the code for second geometrical derivative Coulomb integrals.[32] Due to the limitations of the integral-derivative code in Q-Chem, it cannot handle g and higher angular-momentum functions.

Details for the implementation of the two-electron spin-orbitals within the CFOUR program package[92] can be found in Refs. 93 and 94. We only note here that this implementation follows closely Ref. 95 without use of ladder and projection operator techniques. The integrals are furthermore evaluated directly without computing geometrical integral derivatives as intermediates.

APPENDIX B: PROGRAMMABLE EXPRESSIONS FOR UNSYMMETRIZED DENSITY MATRICES

Because of the symmetry of the spin-orbit integrals, see Eq. (22), one needs to use unsymmetrized (or anti-symmetrized) DMs, contrary to the case of properties and expectation values corresponding to the operators that have symmetric matrix representation such as gradients and dipole moments. In the latter case, symmetrized DMs are commonly used.[86,106,107] The unsymmetrized one- and two-particle DMs are given in the supplementary material.[85]

Since different blocks of γ and Γ are computed separately, Eq. (24) needs to rewritten as follows:

$$\sum_{pq} I_{pq}\gamma_{pq} = \sum_{ij} I_{ij}\gamma_{ij} + \sum_{ia} I_{ia}\gamma_{ia} + \sum_{ai} I_{ai}\gamma_{ai} + \sum_{ab} I_{ab}\gamma_{ab}$$
$$(B1)$$

and

$$\begin{aligned}
\sum_{pqrs} J_{pqrs}\Gamma_{pqrs} = &\sum_{ijkl} J_{ijkl}\Gamma_{ijkl} + \sum_{abcd} J_{abcd}\Gamma_{abcd} \\
&+ \sum_{ijkd} J_{ijkd}\Gamma_{ijkd} + \sum_{ibkl} J_{ibkl}\Gamma_{ibkl} \\
&+ \sum_{ijcl} J_{ijcl}\Gamma_{ijcl} + \sum_{ibkl} J_{ajkl}\Gamma_{ajkl} \\
&+ \sum_{ijcd} J_{ijcd}\Gamma_{ijcd} + \sum_{abkl} J_{abkl}\Gamma_{abkl} \\
&+ \sum_{ibcl} J_{ibcl}\Gamma_{ibcl} + \sum_{ajkd} J_{ajkd}\Gamma_{ajkd} \\
&+ \sum_{ibcd} J_{ibcd}\Gamma_{ibcd} + \sum_{abkd} J_{abkd}\Gamma_{abkd} \\
&+ \sum_{abcl} J_{abcl}\Gamma_{abcl} + \sum_{ajcd} J_{ajcd}\Gamma_{ajcd} \\
&+ \sum_{ajcl} J_{ajcl}\Gamma_{ajcl} + \sum_{ibkd} J_{ibkd}\Gamma_{ibkd}.
\end{aligned}$$
$$(B2)$$

If anti-symmetrized γ and Γ are used, the number of contractions can be reduced.

1. Evaluation of the separable part of the two-electron contribution to SOC

In this section, we derive the spin-integrated equations for the two-particle part of the SOC from Eq. (34). By defining $J(\rho,\gamma) = \sum_{pqrs} J_{pqrs}\rho_{pr}\gamma_{qs}$ and $K(\rho,\gamma) = \sum_{pqrs} J_{pqrs}\rho_{ps}\gamma_{qr}$, Eq. (34) can be rewritten as $-K(\gamma,\rho) + J(\gamma,\rho) - K(\rho,\gamma)$. This gives rise to the following programmable expression for the separable part of two-electron contribution to the SOC:

$$\begin{aligned}
\alpha_x^{2e} = &-2K(\gamma_{\alpha\beta},\rho_\alpha) + J(\gamma_{\alpha\beta},\rho_\alpha) - K(\rho_\alpha,\gamma_{\alpha\beta}) \\
&- 2K(\rho_\alpha,\gamma_{\beta\alpha}) - K(\gamma_{\alpha\beta},\rho_\beta) + J(\gamma_{\alpha\beta},\rho_\beta) \\
&- K(\gamma_{\beta\alpha},\rho_\alpha) + J(\gamma_{\beta\alpha},\rho_\alpha) - 2K(\rho_\beta,\gamma_{\alpha\beta}) \\
&+ J(\gamma_{\beta\alpha},\rho_\beta) - K(\rho_\beta,\gamma_{\beta\alpha}) - 2K(\gamma_{\beta\alpha},\rho_\beta), \\
\alpha_z^{2e} = &-3K(\gamma_{\alpha\alpha},\rho_\alpha) + 3J(\gamma_{\alpha\alpha},\rho_\alpha) - 3K(\rho_\alpha,\gamma_{\alpha\alpha}) \\
&- J(\gamma_{\alpha\alpha},\rho_\beta) + J(\gamma_{\beta\beta},\rho_\alpha) \\
&+ 3K(\gamma_{\beta\beta},\rho_\beta) - 3J(\gamma_{\beta\beta},\rho_\beta) + 3K(\rho_\beta,\gamma_{\beta\beta}).
\end{aligned}$$

In the case of a closed-shell reference $\rho = \rho_\alpha = \rho_\beta$, and therefore the equations reduce to

$$\begin{aligned}
\alpha_x^{2e} = &-3K(\gamma_{\alpha\beta} + \gamma_{\beta\alpha}, \rho) + 2J(\gamma_{\alpha\beta} + \gamma_{\beta\alpha}, \rho) \\
&- 3K(\rho, \gamma_{\alpha\beta} + \gamma_{\beta\alpha}) \\
\alpha_z^{2e} = &-3K(\gamma_{\alpha\alpha} - \gamma_{\beta\beta}, \rho) + 2J(\gamma_{\alpha\alpha} - \gamma_{\beta\beta}, \rho) \\
&- 3K(\rho, \gamma_{\alpha\alpha} - \gamma_{\beta\beta}).
\end{aligned}$$

APPENDIX C: COMPUTING SOCs BETWEEN DIFFERENT MULTIPLET COMPONENTS BY CHANGING THE SPIN-QUANTIZATION AXIS OR THE MOLECULAR ORIENTATION

The determination of the SOCC, Eq. (6), in principle requires calculations for all components of a multiplet. For example, for the SOC calculation in a closed-shell molecule, one needs besides the $M_s = 0$ also the $M_s = \pm 1$ triplet states. However, this need can be circumvented by changing the orientation of the molecule (which is equivalent to changing the spin-quantization axis), which has been, for example, exploited in Ref. 37. Such calculations provide additional means of validating an implementation, as discussed in Sec. III B. Below we describe this strategy by considering a linear molecule as, for example, BH.

The expressions for the SOC given in the Appendix, Eqs. (A7)–(A9), lead to the following selection rules[3] for the SOCs between singlet and triplet states of a linear molecule (such as the S_0/T_1 states of BH):

$$\langle \Psi(s=0, m_s=0)|H^{so}|\Psi'(s=1, m_s=0)\rangle = \langle H_z^{SO}\rangle \equiv h_z,$$
$$(C1)$$

$$\langle \Psi(s=0, m_s=0)|H^{so}|\Psi'(s=1, m_s=+1)\rangle$$
$$= \langle H_x^{SO}\rangle + \langle H_y^{SO}\rangle \equiv \frac{1}{\sqrt{2}}(h_x + h_y), \quad (C2)$$

$$\langle \Psi(s=0, m_s=0)|H^{so}|\Psi'(s=1, m_s=-1)\rangle$$
$$= (\langle \Psi(s=0, m_s=0)|H^{so}|\Psi'(s=1, m_s=1)\rangle)^*. \quad (C3)$$

Thus,

$$|SOCC|^2 = \langle H_z^{SO} \rangle^2 + 2(\langle H_x^{SO} \rangle^2 + \langle H_y^{SO} \rangle^2) = h_x^2 + h_y^2 + h_z^2. \tag{C4}$$

One can compute the couplings between the singlet and the $M_s = \pm 1$ components of the triplet without using the spin-flipped states simply by rotating the molecule (which is equivalent to changing the spin-quantization axis), as was done in Ref. 37. In other words, the quantities defined above can be computed as

$$h_\alpha \equiv \langle \Psi(s = 0, m_s = 0)|H^{so}(\alpha)|\Psi'(s = 1, m_s = 0) \rangle \tag{C5}$$

$$h_i = \frac{1}{\sqrt{2}}(h_j + h_k), \tag{C6}$$

with α as the quantization axis.

[1] D. R. Yarkony, Int. Rev. Phys. Chem. **11**, 195 (1992).
[2] C. M. Marian, Wiley Interdiscip. Rev.: Comput. Mol. Sci. **2**, 187 (2012).
[3] D. G. Fedorov, S. Koseki, M. W. Schmidt, and M. S. Gordon, Int. Rev. Phys. Chem. **22**, 551 (2003).
[4] R. J. Cvetanović, "Addition of Atoms to Olefins in the Gas Phase," in *Advances in Photochemistry*, edited by W. A. Noyes, G. S. Hammond, and J. N. Pitts (1963), Vol. 1, p. 115.
[5] D. L. Singleton, S. Furuyama, R. J. Cvetanović, and R. S. Irwin, J. Chem. Phys. **63**, 1003 (1975).
[6] C. A. Taatjes, D. L. Osborn, T. M. Selby, G. Meloni, A. J. Trevitt, E. Epifanovsky, A. I. Krylov, B. Sirjean, E. Dames, and H. Wang, J. Phys. Chem. A **114**, 3355 (2010).
[7] M. Dupuis, J. J. Wendoloski, T. Takada, and W. A. Lester, J. Chem. Phys. **76**, 481 (1982).
[8] H. Sabbah, L. Biennier, I. A. Sims, Y. Georgievskii, S. J. Klippenstein, and I. W. M. Smith, Science **317**, 102 (2007).
[9] S. Zhao, W. Wu, H. Zhao, H. Wang, C. Yang, K. Liu, and H. Su, J. Phys. Chem. A **113**, 23 (2009).
[10] B. Fu, Y.-C. Han, J. M. Bowman, F. Leonori, N. Balucani, L. Angelucci, A. Occhiogrosso, R. Petrucci, and P. Casavecchia, J. Chem. Phys. **137**, 22A532 (2012).
[11] B. Fu, Y.-C. Han, J. M. Bowman, L. Angelucci, N. Balucani, F. Leonori, and P. Casavecchia, Proc. Natl. Acad. Sci. U. S. A. **109**, 9733 (2012).
[12] T. L. Nguyen, L. Vereecken, X. J. Hou, M. T. Nguyen, and J. Peeters, J. Phys. Chem. A **109**, 7489 (2005).
[13] D. Hodgson, H.-Y. Zhang, M. R. Nimlos, and J. T. McKinnon, J. Phys. Chem. A **105**, 4316 (2001).
[14] T. L. Nguen, J. Peeters, and L. Vereecken, J. Phys. Chem. A **111**, 3836 (2007).
[15] A. C. West, J. D. Lynch, B. Sellner, H. Lischka, W. L. Hase, and T. L. Windus, Theor. Chim. Acta **131**, 1123 (2012).
[16] Q. Cui and K. Morokuma, Theor. Chim. Acta **102**, 127 (1999).
[17] Q. Cui, K. Morokuma, J. M. Bowman, and S. J. Klippenstein, J. Chem. Phys. **110**, 9469 (1999).
[18] R. G. Sadygov and D. R. Yarkony, J. Chem. Phys. **107**, 4994 (1997).
[19] J. C. Tully, J. Chem. Phys. **61**, 61 (1974).
[20] G. E. Zahr, R. K. Preston, and W. H. Miller, J. Chem. Phys. **62**, 1127 (1975).
[21] N. Turro, *Modern Molecular Photochemistry* (Benjamin/Cummings Pub. Co., 1978).
[22] M. Klessinger and J. Michl, *Excited States and Photochemistry of Organic Molecules* (VCH, 1995).
[23] T. Ha and P. Tinnefeld, Annu. Rev. Phys. Chem. **63**, 595 (2012).
[24] Y. Sun, N. C. Giebink, H. Kanno, B. Ma, M. E. Thompson, and S. R. Forrest, Nature **440**, 908 (2006).
[25] M. A. Baldo, S. P. Forrest, and M. E. Thompson, Org. Electroluminescence **94**, 267 (2005).
[26] A. Tajti, P. G. Szalay, A. G. Császár, M. Kállay, J. Gauss, E. F. Valeev, B. A. Flowers, J. Vázquez, and J. F. Stanton, J. Chem. Phys. **121**, 11599 (2004).
[27] H. A. Bethe and E. E. Salpeter, *Quantum Mechanics of One and Two Electron Atoms* (Plenum, New York, 1977).
[28] *Relativistic Electronic Structure Theory*, edited by P. Schwerdtfeger (Elsevier, Amsterdam, 2002).
[29] H. Ågren, O. Vahtras, and B. Minaev, "Response theory and calculations of spin-orbit coupling phenomena in molecules," in *Advances in Quantum Chemistry* (Academic Press, 1996), Vol. 27, pp. 71–162.
[30] B. A. Hess, C. M. Marian, U. Wahlgren, and O. Gropen, Chem. Phys. Lett. **251**, 365 (1996).
[31] T. R. Furlani and H. F. King, J. Chem. Phys. **82**, 5577 (1985).
[32] H. F. King and T. R. Furlani, J. Comput. Chem. **9**, 771 (1988).
[33] D. G. Fedorov and M. S. Gordon, J. Chem. Phys. **112**, 5611 (2000).
[34] O. Vahtras, H. Ågren, P. Jørgensen, H. J. Aa. Jensen, T. Helgaker, and J. Olsen, J. Chem. Phys. **96**, 2118 (1992).
[35] A. Berning, M. Schweizer, H.-J. Werner, P. Knowles, and P. Palmieri, Mol. Phys. **98**, 1823 (2000).
[36] F. Neese, J. Chem. Phys. **122**, 034107 (2005).
[37] O. Christiansen, J. Gauss, and B. Schimmelpfennig, Phys. Chem. Chem. Phys. **2**, 965 (2000).
[38] K. Klein and J. Gauss, J. Chem. Phys. **129**, 194106 (2008).
[39] L. A. Mück, "Highly accurate quantum chemistry: Spin-orbit splittings via multireference coupled-cluster methods and applications in heavy-atom main-group chemistry," Ph.D. thesis, Johannes-Gutenberg Universität Mainz, 2013.
[40] L. A. Mück and J. Gauss, J. Chem. Phys. **136**, 111103 (2012).
[41] S. G. Chiodo and N. Russo, Chem. Phys. Lett. **490**, 90 (2010).
[42] Z. Li, B. Suo, Y. Zhang, Y. Xiao, and W. Liu, Mol. Phys. **111**, 3741 (2013).
[43] Z. Tu, F. Wang, and X. Li, J. Chem. Phys. **136**, 174102 (2012).
[44] D.-D. Yang, F. Wang, and J. Guo, Chem. Phys. Lett. **531**, 236 (2012).
[45] Z. Wang, Z. Tu, and F. Wang, J. Chem. Theory Comput. **10**, 5567 (2014).
[46] H. E. Zimmerman and A. G. Kutateladze, J. Am. Chem. Soc. **118**, 249 (1996).
[47] L. Salem and C. Rowland, Angew. Chem., Int. Ed. Engl. **11**, 92 (1972).
[48] R. J. Bartlett, Annu. Rev. Phys. Chem. **32**, 359 (1981).
[49] R. J. Bartlett and J. F. Stanton, Rev. Comput. Chem. **5**, 65 (1994).
[50] R. J. Bartlett, Int. J. Mol. Sci. **3**, 579 (2002).
[51] A. I. Krylov, Annu. Rev. Phys. Chem. **59**, 433 (2008).
[52] R. J. Bartlett, Mol. Phys. **108**, 2905 (2010).
[53] K. Sneskov and O. Christiansen, Wiley Interdiscip. Rev.: Comput. Mol. Sci. **2**, 566 (2012).
[54] R. J. Bartlett, Wiley Interdiscip. Rev.: Comput. Mol. Sci. **2**, 126 (2012).
[55] H. Reisler and A. I. Krylov, Int. Rev. Phys. Chem. **28**, 267 (2009).
[56] P. A. Pieniazek, S. A. Arnstein, S. E. Bradforth, A. I. Krylov, and C. D. Sherrill, J. Chem. Phys. **127**, 164110 (2007).
[57] A. I. Krylov, Acc. Chem. Res. **39**, 83 (2006).
[58] E. P. Wigner, *Group Theory* (Academic Press, New York, 1959).
[59] C. Eckart, Rev. Mod. Phys. **2**, 305 (1930).
[60] A. I. Krylov, Chem. Phys. Lett. **338**, 375 (2001).
[61] S. V. Levchenko and A. I. Krylov, J. Chem. Phys. **120**, 175 (2004).
[62] M. Wladyslawski and M. Nooijen, "The photoelectron spectrum of the NO₃ radical revisited: A theoretical investigation of potential energy surfaces and conical intersections," in *ACS Symposium Series* (American Chemical Society, 2002), Vol. 828, pp. 65–92.
[63] M. Nooijen, Int. J. Mol. Sci. **3**, 656 (2002).
[64] K. W. Sattelmeyer, H. F. Schaefer, and J. F. Stanton, Chem. Phys. Lett. **378**, 42 (2003).
[65] M. Musiał, A. Perera, and R. J. Bartlett, J. Chem. Phys. **134**, 114108 (2011).
[66] T. Kuś and A. I. Krylov, J. Chem. Phys. **135**, 084109 (2011).
[67] T. Kuś and A. I. Krylov, J. Chem. Phys. **136**, 244109 (2012).
[68] J. Shen and P. Piecuch, J. Chem. Phys. **138**, 194102 (2013).
[69] J. Shen and P. Piecuch, Mol. Phys. **112**, 868 (2014).
[70] H. J. Monkhorst, Int. J. Quantum Chem. **11**, 421 (1977).
[71] D. Mukherjee and P. K. Mukherjee, Chem. Phys. **39**, 325 (1979).
[72] H. Sekino and R. J. Bartlett, Int. J. Quantum Chem. **26**, 255 (1984).
[73] H. Koch, H. J. Aa. Jensen, P. Jørgensen, and T. Helgaker, J. Chem. Phys. **93**, 3345 (1990).
[74] M. Head-Gordon and T. J. Lee, "Single reference coupled cluster and perturbation theories of electronic excitation energies," in *Modern Ideas in Coupled Cluster Theory*, edited by R. J. Bartlett (World Scientific, Singapore, 1997).
[75] The reference determines the separation of the orbital space into the occupied and virtual subspaces. Here, we use indices $i, j, k, \ldots$ and $a, b, c, \ldots$ to denote the orbitals from the two subspaces. To denote orbitals that can be either occupied or virtual, the letters $p, q, r, s, \ldots$ will be used.
[76] S. Koseki, M. Schmidt, and M. S. Gordon, J. Phys. Chem. **96**, 10768 (1992).
[77] T. Helgaker, S. Coriani, P. Jørgensen, K. Kristensen, J. Olsen, and K. Ruud, Chem. Rev. **112**, 543 (2012).
[78] P. B. Rozyczko, S. A. Perera, M. Nooijen, and R. J. Bartlett, J. Chem. Phys. **107**, 6736 (1997).
[79] M. Kállay and J. Gauss, J. Mol. Struct.: THEOCHEM **768**, 71 (2006).

[80]D. P. O'Neill, M. Kállay, and J. Gauss, J. Chem. Phys. **127**, 134109 (2007).

[81]J. F. Stanton and R. J. Bartlett, J. Chem. Phys. **98**, 7029 (1993).

[82]K. Nanda and A. I. Krylov, J. Chem. Phys. **142**, 064118 (2015).

[83]J. F. Stanton, J. Chem. Phys. **101**, 8928 (1994).

[84]R. Kobayashi, H. Koch, and P. Jørgensen, Chem. Phys. Lett. **219**, 30 (1994).

[85]See supplementary material at http://dx.doi.org/10.1063/1.4927785 for additional details. This document can be reached through a direct link in the online article, HTML reference section or via the EPAPS homepage (http://www.aip.org/pubservs/epaps.html).

[86]S. V. Levchenko, T. Wang, and A. I. Krylov, J. Chem. Phys. **122**, 224106 (2005).

[87]For a state property, this expression needs to be modified as follows: $\alpha^{2e} = \frac{1}{2} \sum_{pq} \left(\gamma_{pq} - \frac{1}{2} \rho_{pq} \right) \left[\sum_{rs} \rho_{rs} \left(A_{prqs} + A_{rpsq} - A_{prsq} - A_{rpqs} \right) \right]$.

[88]X. Feng, A. V. Luzanov, and A. I. Krylov, J. Phys. Chem. Lett. **4**, 3845 (2013).

[89]S. Matsika, X. Feng, A. V. Luzanov, and A. I. Krylov, J. Phys. Chem. A **118**, 11943 (2014).

[90]B. Schimmelpfennig, AMFI, an atomic mean-field spin-orbit integral program, University of Stockholm, 1996.

[91]Y. Shao, Z. Gan, E. Epifanovsky, A. T. B. Gilbert, M. Wormit, J. Kussmann, A. W. Lange, A. Behn, J. Deng, X. Feng, D. Ghosh, M. Goldey, P. R. Horn, L. D. Jacobson, I. Kaliman, R. Z. Khaliullin, T. Kus, A. Landau, J. Liu, E. I. Proynov, Y. M. Rhee, R. M. Richard, M. A. Rohrdanz, R. P. Steele, E. J. Sundstrom, H. L. Woodcock III, P. M. Zimmerman, D. Zuev, B. Albrecht, E. Alguires, B. Austin, G. J. O. Beran, Y. A. Bernard, E. Berquist, K. Brandhorst, K. B. Bravaya, S. T. Brown, D. Casanova, C.-M. Chang, Y. Chen, S. H. Chien, K. D. Closser, D. L. Crittenden, M. Diedenhofen, R. A. DiStasio, Jr., H. Do, A. D. Dutoi, R. G. Edgar, S. Fatehi, L. Fusti-Molnar, A. Ghysels, A. Golubeva-Zadorozhnaya, J. Gomes, M. W. D. Hanson-Heine, P. H. P. Harbach, A. W. Hauser, E. G. Hohenstein, Z. C. Holden, T.-C. Jagau, H. Ji, B. Kaduk, K. Khistyaev, J. Kim, J. Kim, R. A. King, P. Klunzinger, D. Kosenkov, T. Kowalczyk, C. M. Krauter, K. U. Laog, A. Laurent, K. V. Lawler, S. V. Levchenko, C. Y. Lin, F. Liu, E. Livshits, R. C. Lochan, A. Luenser, P. Manohar, S. F. Manzer, S.-P. Mao, N. Mardirossian, A. V. Marenich, S. A. Maurer, N. J. Mayhall, C. M. Oana, R. Olivares-Amaya, D. P. O'Neill, J. A. Parkhill, T. M. Perrine, R. Peverati, P. A. Pieniazek, A. Prociuk, D. R. Rehn, E. Rosta, N. J. Russ, N. Sergueev, S. M. Sharada, S. Sharmaa, D. W. Small, A. Sodt, T. Stein, D. Stuck, Y.-C. Su, A. J. W. Thom, T. Tsuchimochi, L. Vogt, O. Vydrov, T. Wang, M. A. Watson, J. Wenzel, A. White, C. F. Williams, V. Vanovschi, S. Yeganeh, S. R. Yost, Z.-Q. You, I. Y. Zhang, X. Zhang, Y. Zhou, B. R. Brooks, G. K. L. Chan, D. M. Chipman, C. J. Cramer, W. A. Goddard III, M. S. Gordon, W. J. Hehre, A. Klamt, H. F. Schaefer III, M. W. Schmidt, C. D. Sherrill, D. G. Truhlar, A. Warshel, X. Xu, A. Aspuru-Guzik, R. Baer, A. T. Bell, N. A. Besley, J.-D. Chai, A. Dreuw, B. D. Dunietz, T. R. Furlani, S. R. Gwaltney, C.-P. Hsu, Y. Jung, J. Kong, D. S. Lambrecht, W. Z. Liang, C. Ochsenfeld, V. A. Rassolov, L. V. Slipchenko, J. E. Subotnik, T. Van Voorhis, J. M. Herbert, A. I. Krylov, P. M. W. Gill, and M. Head-Gordon, Mol. Phys. **113**, 184 (2015).

[92]J. F. Stanton, J. Gauss, M. E. Harding, and P. G. Szalay, with contributions from A. A. Auer, R. J. Bartlett, U. Benedikt, C. Berger, D. E. Bernholdt, Y. J. Bomble, L. Cheng, O. Christiansen, M. Heckert, O. Heun, C. Huber, T.-C. Jagau, D. Jonsson, J. Jusélius, K. Klein, W. J. Lauderdale, F. Lipparini, D. A. Matthews, T. Metzroth, L. A. Mück, D. P. O'Neill, D. R. Price, E. Prochnow, C. Puzzarini, K. Ruud, F. Schiffmann, W. Schwalbach, C. Simmons, S. Stopkowicz, A. Tajti, J. Vázquez, F. Wang, and J. D. Watts; and the integral packages MOLECULE (J. Almlöf and P. R. Taylor), PROPS (P. R. Taylor), ABACUS (T. Helgaker, H. J. Aa. Jensen, P. Jørgensen, and J. Olsen), and ECP routines by A. V. Mitin and C. van Wüllen. For the current version, see http://www.cfour.de.

[93]S. Stopkowicz, "Higher-order perturbative relativistic corrections to energies and properties," Ph.D. thesis, Johannes-Gutenberg Universität Mainz, 2011.

[94]S. Stopkowicz and J. Gauss, J. Chem. Phys. **134**, 064114 (2011).

[95]L. E. McMurchie and E. R. Davidson, J. Chem. Phys. **26**, 218 (1978).

[96]J. F. Stanton and J. Gauss, Theor. Chim. Acta **91**, 267 (1995).

[97]J. F. Stanton and J. Gauss, J. Chem. Phys. **101**, 8938 (1994).

[98]J. F. Stanton and J. Gauss, J. Chem. Phys. **100**, 4695 (1994).

[99]M. A. El-Sayed, Acc. Chem. Res. **1**, 8 (1968).

[100]Z. Havlas, J. W. Downing, and J. Michl, J. Phys. Chem. A **102**, 5681 (1998).

[101]J. S. Sears, C. D. Sherrill, and A. I. Krylov, J. Chem. Phys. **118**, 9084 (2003).

[102]L. V. Slipchenko and A. I. Krylov, J. Chem. Phys. **117**, 4694 (2002).

[103]S. Huzinaga and B. Miguel, Chem. Phys. Lett. **175**, 289 (1990).

[104]S. H. Kable, S. A. Reid, and T. J. Sears, Int. Rev. Phys. Chem. **28**, 435 (2009).

[105]S. Nyambo, C. Karshenas, S. A. Reid, P. Lolur, and R. Dawes, J. Chem. Phys. **142**, 214304 (2015).

[106]C. D. Sherrill, A. I. Krylov, E. F. C. Byrd, and M. Head-Gordon, J. Chem. Phys. **109**, 4171 (1998).

[107]A. I. Krylov, C. D. Sherrill, and M. Head-Gordon, J. Chem. Phys. **113**, 6509 (2000).